Mineralogical Magazine, February 2018, Vol. 82(1), pp. 59–88

Trace elements in hydrothermal chalcopyrite

LUKE L. GEORGE[1,*], NIGEL J. COOK[2], BRYONY B. P. CROWE[1] AND CRISTIANA L. CIOBANU[2]

[1] School of Physical Sciences, University of Adelaide, Adelaide S.A. 5005, Australia
[2] School of Chemical Engineering, University of Adelaide, Adelaide S.A. 5005, Australia

[*Received 1 July 2016; Accepted 27 March 2017; Associate Editor: Brian O'Driscoll*]

ABSTRACT

Concentration data are reported for 18 trace elements in chalcopyrite from a suite of 53 samples from 15 different ore deposits obtained by laser-ablation inductively-coupled plasma-mass spectrometry. Chalcopyrite is demonstrated to host a wide range of trace elements including Mn, Co, Zn, Ga, Se, Ag, Cd, In, Sn, Sb, Hg, Tl, Pb and Bi. The concentration of some of these elements can be high (hundreds to thousands of ppm) but most are typically tens to hundreds of ppm. The ability of chalcopyrite to host trace elements generally increases in the absence of other co-crystallizing sulfides. In deposits in which the sulfide assemblage recrystallized during syn-metamorphic deformation, the concentrations of Sn and Ga in chalcopyrite will generally increase in the presence of co-recrystallizing sphalerite and/or galena, suggesting that chalcopyrite is the preferred host at higher temperatures and/or pressures. Trace-element concentrations in chalcopyrite typically show little variation at the sample scale, yet there is potential for significant variation between samples from any individual deposit. The Zn:Cd ratio in chalcopyrite shows some evidence of a systematic variation across the dataset, which depends, at least in part, on temperature of crystallization. Under constant physiochemical conditions the Cd:Zn ratios in co-crystallizing chalcopyrite and sphalerite are typically approximately equal. Any distinct difference in the Cd:Zn ratios in the two minerals, and/or a non-constant Cd:Zn ratio in chalcopyrite, may be an indication of varying physiochemical conditions during crystallization.

Chalcopyrite is generally a poor host for most elements considered harmful or unwanted in the smelting of Cu, suggesting it is rarely a significant contributor to the overall content of such elements in copper concentrates. The exceptions are Se and Hg which may be sufficiently enriched in chalcopyrite to exceed statutory limits and thus incur monetary penalties from a smelter.

KEYWORDS: chalcopyrite, trace elements, substitution controls, penalty elements.

Introduction

CHALCOPYRITE is the principal ore mineral of copper (Geoscience Australia, 2015). Concentrates produced from chalcopyrite-rich ores may also be enriched significantly in other elements. Silver is one such element and is commonly extracted as an economic by-product during copper smelting and refining (Ayres *et al.*, 2013). Other elements, including As, Sb, Hg, Bi and Se, may become enriched in copper concentrates during ore processing and can, if present at high enough concentrations, result in substantial financial penalties when sold on the world market (e.g. Fountain, 2013). Yet, regardless of the importance of chalcopyrite in the minerals industry, there is a relative lack of understanding as to the different trace elements chalcopyrite can accommodate into its structure, as well as the ranges of concentration of these elements.

Detailed studies addressing trace-element concentrations in chalcopyrite are relatively scarce when compared to other common sulfide minerals, notably pyrite (e.g. Huston *et al.*, 1995; Large *et al.*, 2009; Winderbaum *et al.*, 2012; Belousov *et al.*, 2016), or sphalerite and galena (e.g. Bethke and Barton, 1971; Blackburn and Schwendeman, 1977; Johan, 1988; Foord and

*E-mail: luke.george@adelaide.edu.au
https://doi.org/10.1180/minmag.2017.081.021

Shawe, 1989; Cook *et al.*, 2009; George *et al.*, 2015). Much of the published data for chalcopyrite (e.g. Harris *et al.*, 1984; Cabri *et al.*, 1985; Kase, 1987; Brill, 1989; Huston *et al.*, 1996; Scott *et al.*, 2001; Moggi-Cecchi *et al.*, 2002; Serranti *et al.*, 2002; Shalaby *et al.*, 2004; Demir *et al.*, 2008; Layton-Matthews *et al.*, 2008; Monteiro *et al.*, 2008; Demir *et al.*, 2013; Gena *et al.*, 2013; Reich *et al.*, 2013; Cioacă *et al.*, 2014; Helmy *et al.*, 2014; Wang *et al.*, 2015*a*; Wohlgemuth-Ueberwasser *et al.*, 2015; Sadati *et al.*, 2016) is focused on a limited suite of trace elements, and commonly the minimum detection limits of the microanalytical techniques used are too high to actually establish trace-element diversity and concentration levels.

More work is thus necessary to establish the ability of chalcopyrite to host trace elements in a wide range of environments and settings. With this objective in mind, we used laser-ablation inductively-coupled plasma mass spectrometry (LA-ICP-MS) to determine the concentration ranges of 18 trace elements (elements typically present at concentrations < 1 wt.%) in natural hydrothermal chalcopyrite from a diverse suite of 53 samples from different ore types, settings and environments, and physiochemical conditions of ore formation. The trace-element chemistry of chalcopyrite in deposits of magmatic origin is not part of this study. A number of studies on the topic have been published, enabling a sound understanding of trace-element partitioning in chalcopyrite-bearing magmatic ores (e.g. Barnes *et al.*, 2006; Holwell and McDonald, 2007; Godel and Barnes, 2008; Dare *et al.*, 2010; Djon and Barnes, 2012; Piña *et al.*, 2012; Prichard *et al.*, 2013; Chen *et al.*, 2014; Duran *et al.*, 2015; Barnes and Ripley, 2016; Smith *et al.*, 2016). The LA-ICP-MS technique offers both sub-part-per-million-level precision for many heavier elements and micrometre-scale spatial resolution. Laser-ablation ICP-MS may also reveal the presence of micro-inclusions within the analysed spot because if they are large enough and distributed heterogeneously, they are recognizable on time-resolved downhole spectra (e.g. George *et al.*, 2015). The dataset reveals chalcopyrite to be an important trace-element carrier in many ore deposits. Our data carries implications for both ore genesis and mineral processing. We also show that the Cd:Zn ratio in chalcopyrite (and co-existing sphalerite) may assist in determining if physiochemical conditions remained constant during base-metal sulfide crystallization.

Background

Chalcopyrite crystal structure

Chalcopyrite crystallizes in a body-centred tetragonal lattice system with tetrahedrally-coordinated Cu, Fe and S atoms. Both Cu and Fe are ordered into the cation sites. Pauling and Brockway (1932) regarded the bonding between atoms in the chalcopyrite structure as effectively covalent with valencies of Cu and Fe atoms fluctuating between monovalent-divalent, and divalent-trivalent, respectively. The strong covalent nature of chalcopyrite was also affirmed by Donnay *et al.* (1958). Similarly, Hall and Stewart (1973) argued for a strong covalent configuration with an effective ionic state between $Cu^{+}Fe^{3+}S_2^{2-}$ and $Cu^{2+}Fe^{2+}S_2^{2-}$ Nevertheless, for the sake of convenience, chalcopyrite is generally represented with ions of specific valencies, i.e. $Cu^{+}Fe^{3+}S_2^{2-}$.

Regardless, Todd and Sherman (2003), Todd *et al.* (2003) and Mikhlin *et al.* (2005) have argued, on the basis of X-ray absorption spectroscopy (XAS) and X-ray absorption near-edge structure (XANES) spectra, that the nominal valencies in chalcopyrite should be $Cu^{2+}Fe^{2+}S_2^{2-}$. This was rejected by Pearce *et al.* (2006), who affirmed that Cu in chalcopyrite is nominally monovalent, and that Fe is nominally trivalent. Nominally divalent character in copper sulfides is very rare, and energy peaks associated with Cu^{2+} can be explained by contamination by Cu^{2+} species. Li *et al.* (2013) confirmed that evidence for the presence of Cu^{2+} and Fe^{2+} has been largely discredited, but emphasizes that the actual valence state of chalcopyrite should be understood as intermediate between $Cu^{+}Fe^{3+}S_2^{2-}$ and $Cu^{2+}Fe^{2+}S_2^{2-}$ due to covalent bonding.

Previous trace-element data

A number of previous studies addressed the composition of natural chalcopyrite, yet most of these had purposes other than to establish if chalcopyrite is a good host for trace elements. Chalcopyrite from various locations has been described by Kase (1987), Brill (1989), Scott *et al.* (2001), Serranti *et al.* (2002), Shalaby *et al.* (2004), Demir *et al.* (2008), Layton-Matthews *et al.* (2008), Monteiro *et al.* (2008), Demir *et al.* (2013), Gena *et al.* (2013), Cioacă *et al.* (2014), Helmy *et al.* (2014), Wang *et al.* (2015*a*) and Sadati *et al.* (2016). However, in each case, only electron probe microanalysis (EPMA) is used to determine

https://doi.org/10.1180/minmag.2017.081.021 Published online by Cambridge University Press

chalcopyrite composition. With minimum detection limits in the order of hundreds of ppm unless exceptionally long count times are used, EPMA is not an adequate technique for determining many trace-element abundances. Harris *et al.* (1984), Cabri *et al.* (1985), Huston *et al.* (1996) and Moggi-Cecchi *et al.* (2002) used a proton microprobe, Reich *et al.* (2013) used secondary ion mass spectrometry (SIMS) and Wohlgemuth-Ueberwasser *et al.* (2015) used LA-ICP-MS to investigate chalcopyrite from different localities. While these analytical techniques boast minimum detection limits significantly lower than EPMA, none of these studies reported data for more than six elements. The elements reported are typically common trace constituents, so few inferences about the presence of other trace elements could be drawn. Chalcopyrite compositions were determined by Bajwah *et al.* (1987), Butler and Nesbitt (1999) and Ulrich *et al.* (2002) by atomic absorption spectroscopy (AAS), solution ICP-MS and ICP optical emission spectrometry (OES), respectively. These techniques remain bulk methods and so are limited in their ability to determine lattice bound trace constituents with confidence. Other studies such as Subba Rao and Naqvi (1997), McClenaghan *et al.* (2009), Cook *et al.* (2011) and Maydagán *et al.* (2013) only measured chalcopyrite in a limited number of samples (maximum of four), as they primarily focused on characterizing the chemistry of complex phase assemblages. The different emphasis of such studies highlights the need for a more detailed investigation of a larger, more diverse sample suite, considering a wider range of potential trace elements, and utilizing an analytical technique with low minimum detection limits. We acknowledge that the spectrum of elements analysed in chalcopyrite has been somewhat restricted by the availability of appropriate matrix-matched standards, particularly with respect to some chalcophile semi-metals, and thus data quality remains, to this day, better for some elements than for others (e.g. Se, As, Au).

Regardless of their limitations, the prior studies cited above, and indeed other more thorough investigations of chalcopyrite composition (e.g. Huston *et al.*, 1995; Maslennikov *et al.*, 2009; Revan *et al.*, 2014; Wang *et al.*, 2015*b*; George *et al.*, 2016), provide a valuable background for understanding chalcopyrite as a trace-element carrier and serve as a broad foundation for the present study. The maximum reported concentrations of various trace elements in chalcopyrite from different deposit types is summarized in Table 1.

Silver is the trace element most commonly reported in chalcopyrite. Shalaby *et al.* (2004) described unusual green chalcopyrite from the Um Samiuki volcanogenic massive sulfide (VMS) deposit, Egypt, hosting up to 4.3 wt.% Ag. More typically, concentrations are in the tens to hundreds of ppm range, although sometimes reaching into the thousands, for example from the Izok Lake Zn-Cu-Pb deposit, Northwest Territories, Canada (Harris *et al.*, 1984), the Kidd Creek mine, Ontario, Canada (Cabri *et al.*, 1985), the Bottino Mine, Italy (Moggi-Cecchi *et al.*, 2002), and Mantos Blancos, northern Chile (Reich *et al.*, 2013).

Experiments in the Cu-Fe-Zn-S system have revealed that chalcopyrite may dissolve up to 0.9 at.% zinc at 500°C, 0.8 at.% at 400°C and 0.6 at.% at 300°C (Kojima and Sugaki, 1985). Indeed Huston *et al.* (1995) measured Zn in chalcopyrite from Australian volcanic-hosted massive sulfide (VHMS) deposits at concentrations from below the minimum detection limit up to as much as 5 wt.%. They concluded that concentrations up to 2000 ppm probably reflect Zn in solid solution (substituted for Fe), but that concentrations exceeding 2000 ppm Zn are probably the result of micro-inclusions of sphalerite. Moggi-Cecchi *et al.* (2002) also concluded that high distributions of Zn in chalcopyrite from Italian and Slovak deposits are related predominantly to micro-scale inclusions of Zn-bearing phases. Nevertheless, large Zn values of 1.86 wt.%, 1.83 wt.%, 1.73 wt.% and 1.64 wt.% have been measured in chalcopyrite by Shalaby *et al.* (2004), Helmy *et al.* (2014), Serranti *et al.* (2002) and Wang *et al.* (2015*a*), respectively, and have not been attributed, in any of these cases, to inclusion-related Zn.

Huston *et al.* (1995) measured arsenic in chalcopyrite from Australian VHMS deposits into the thousands of ppm. These high concentrations of As could not readily be attributed to micro-inclusions of distinct As-bearing phases and it was concluded that As can substitute into the chalcopyrite lattice up to ~2000 ppm. Scott *et al.* (2001) and Wang *et al.* (2015*a*) reported chalcopyrite containing up to 1600 ppm As from Woodlawn, New South Wales, Australia, and the Xiaozhen Cu deposit, Shaanxi Province, China, respectively.

Bethke and Barton (1971) showed that chalcopyrite could accommodate as much as 0.5 mol.% eskebornite ($CuFeSe_2$) at 390°C, and thus may be a significant host of selenium. Cabri *et al.* (1985) reported as much as 0.46 wt.% Se in chalcopyrite

https://doi.org/10.1180/minmag.2017.081.021 Published online by Cambridge University Press

TABLE 1. Maximum reported trace-element contents of chalcopyrite by deposit type as reported in the literature.

Deposit type	Mn		Co		Ni		Zn	
Epithermal	43 ppm	George *et al.* (2016)	3.3 ppm	George *et al.* (2016)	–		1.6 wt.%	Demir *et al.* (2008)
Skarn	540 ppm	Bajwah *et al.* (1987)	7500 ppm	Bajwah *et al.* (1987)	925 ppm	Bajwah *et al.* (1987)	1.83 wt.%	Helmy *et al.* (2014)
Porphyry	0.02 wt.%	Maydagan *et al.* (2013)	249 ppm	Cioacă *et al.* (2014)	9 ppm	Maydagan *et al.* (2013)	0.22 wt.%	Maydagan *et al.* (2013)
Exhalative	642 ppm	Revan *et al.* (2014)	40 ppm	Maslennikov *et al.* (2009)	3.2 ppm	Maslennikov *et al.* (2009)	810 ppm	Huston *et al.* (1995)
Recrystallized exhalative	196 ppm	George *et al.* (2016)	2720 ppm	Thole (1976)	3300 ppm	Thole (1976)	1.86 wt.%	Shalaby *et al.* (2004)
Deposit type	Ga		As		Se		Ag	
Epithermal	1.3 ppm	George *et al.* (2016)	0.73 ppm	George *et al.* (2016)	300 ppm	Moggi-Cecchi *et al.* (2002)	630 ppm	Moggi-Cecchi *et al.* (2002)
Skarn	0.23 ppm	George *et al.* (2016)	0.54 ppm	George *et al.* (2016)	538 ppm	Cook *et al.* (2011)	0.3 wt.%	Helmy *et al.* (2014)
Porphyry	–		0.05 wt.%	Maydagan *et al.* (2013)	0.03 wt.%	Rubin and Kyle (1997)	0.05 wt.%	Maydagan *et al.* (2013)
Exhalative	0.13 ppm	George *et al.* (2016)	282 ppm	Maslennikov *et al.* (2009)	0.46 wt.%	Cabri *et al.* (1985)	0.19 wt.%	Cabri *et al.* (1985)
Recrystallized exhalative	16 ppm	George *et al.* (2016)	2,000 ppm	Huston *et al.* (1995)	480 ppm	Serranti *et al.* (2002)	4.3 wt.%	Shalaby *et al.* (2004)
Deposit type	Cd		In		Sn		Sb	
Epithermal	24 ppm	George *et al.* (2016)	14 ppm	George *et al.* (2016)	2.3 wt.%	Kase, 1987)	4.2 ppm	George *et al.* (2016)
Skarn	25 ppm	Bajwah *et al.* (1987)	2214 ppm	Andersen *et al.* (2016)	47 ppm	George *et al.* (2016)	0.28 ppm	George *et al.* (2016)
Porphyry	0.55 ppm	Maydagan *et al.* (2013)	–		122 ppm	Maydagan *et al.* (2013)	0.1 wt.%	Maydagan *et al.* (2013)
Exhalative	10 ppm	Huston *et al.* (1995	1119 ppm	Cabri *et al.* (1985	1345 ppm	Cabri *et al.* (1985)	488 ppm	Maslennikov *et al.* (2009)
Recrystallized exhalative	77 ppm	Serranti *et al.* (2002	100 ppm	Huston *et al.* (1995	2940 ppm	Huston *et al.* (1995)	31 ppm	McClenaghan *et al.* (2009)
Deposit type	Te		Au		Hg		Tl	
Epithermal	0.04 ppm	George *et al.* (2016)	–		95 ppm	George *et al.* (2016)	0.01 ppm	George *et al.* (2016)
Skarn	6.6 ppm	Cook *et al.* (2011)	0.2 ppm	Cook *et al.* (2011)	2.9 ppm	George *et al.* (2016)	0.03 ppm	Cook *et al.* (2011)
Porphyry	306 ppm	Cioacă *et al.* (2014)	0.05 ppm	Maydagan *et al.* (2013)	–		–	
Exhalative	7447 ppm	Maslennikov *et al.* (2009	7.73 ppm	Maslennikov *et al.* (2009	32 ppm	George *et al.* (2016)	1 ppm	Maslennikov *et al.* (2009)
Recrystallized exhalative	0.05 ppm	George *et al.* (2016)	0.16 ppm	McClenaghan *et al.* (2009	2.3 ppm	McClenaghan *et al.* (2009)	0.14 ppm	George *et al.* (2016)

Deposit type	Pb		Bi	
Epithermal	630 ppm	Moggi-Cecchi *et al.* (2002)	0.05 ppm	George *et al.* (2016)
Skarn	175 ppm	Bajwah *et al.* (1987)	37.9 ppm	Cook *et al.* (2011)
Porphyry	0.17 wt.%	Maydagan *et al.* (2013)	0.53 ppm	Maydagan *et al.* (2013)
Exhalative	2943 ppm	Maslennikov *et al.* (2009)	1353 ppm	Maslennikov *et al.* (2009)
Recrystallized exhalative	287 ppm	Ulrich *et al.* (2002)	0.07 ppm	McClenaghan *et al.* (2009)

Only anomalous reports that have obviously been influenced by micro-inclusions are excluded. Other reports may still be influenced by micro-inclusions. The literature review was thorough, though not exhaustive.

from Kidd Creek, Ontario, Canada, while Monteiro *et al.* (2008) and Wang *et al.* (2015*a*) each recorded over 2000 ppm Se in chalcopyrite from Xiaozhen, China, and Sossego, Brazil, respectively.

Exceptional reports of cobalt and nickel in chalcopyrite suggest that the Cu-sulfide may, on rare occasions, be a good host for Co and Ni. Bajwah *et al.* (1987) documented chalcopyrite from Big Cadia, New South Wales, Australia, which hosted up to 7500 ppm Co and 925 ppm Ni. Thole (1976) recorded up to 2700 ppm Co and 3300 ppm Ni in chalcopyrite from the Shamrocke mine, Zimbabwe. Wang *et al.* (2015*a*) measured up to 1700 ppm Co and 4100 ppm Ni in chalcopyrite from the Xiaozhen Cu deposit, Shaanxi Province, China, while Wang *et al.* (2015*b*) also reported chalcopyrite containing 6178 ppm Co and 2496 ppm Ni from the Shilu Fe-Co-Cu ore district in the Hainan Province of South China.

Lead concentrations in chalcopyrite are uncommonly reported in the thousands of ppm, though such high concentrations are probably the result of micro-inclusions of Pb-bearing phases, commonly galena. Among such anomalous reports are 7054 ppm Pb in chalcopyrite from Yaman-Kasy, Russia (Maslennikov *et al.*, 2009), and 0.34 wt.% Pb in chalcopyrite from the Xiaozhen Cu deposit, Shaanxi Province, China (Wang *et al.*, 2015*a*). Maximum reported Pb concentrations in chalcopyrite are ordinarily in the hundreds of ppm (e.g. Bajwah *et al.*, 1987; Moggi-Cecchi *et al.*, 2002).

High levels of bismuth and tellurium are measured in chalcopyrite from active seafloor hydrothermal systems. Gena *et al.* (2013) recorded up to 0.32 wt.% Bi in chalcopyrite associated with bismuthinite from the Tiger sulfide chimney, Southern okinawa Trough, Japan, while 45 ppm Te was measured in chalcopyrite from the Broken Spur vent field by Butler and Nesbitt (1999). Nevertheless, chalcopyrite is generally a poor host of both elements with reported concentrations from ore deposits rarely exceeding 10 ppm (e.g. Maydagán *et al.*, 2013; George *et al.*, 2016).

Chalcopyrite may contain at most up to a few ppm gold. Synthetic experiments carried out by Simon *et al.* (2000) showed that up to 16 ppm Au is soluble in chalcopyrite at 500°C, decreasing to 4 ppm at 400°C. Reports of chalcopyrite hosting hundreds of even thousands of ppm Au are almost certainly related to Au-bearing mineral inclusions (e.g. Maslennikov *et al.*, 2009). Nevertheless some studies have reported tens of ppm Au in chalcopyrite (e.g. Revan *et al.*, 2014).

https://doi.org/10.1180/minmag.2017.081.021 Published online by Cambridge University Press

Although there are some rare reports of thousands of ppm antimony and cadmium in chalcopyrite (e.g. Revan *et al.*, 2014), concentrations rarely reach into the hundreds of ppm. Monteiro *et al.* (2008) measured up to 330 ppm Sb in chalcopyrite from the Sossego IOCG deposit, Brazil, and up to 77 ppm Cd have been reported from Arinteiro, Galicia, Spain (Serranti *et al.*, 2002).

Over 2.3 wt.% tin has been measured in chalcopyrite from the Izumo vein, Toyoha mine, Japan (Kase, 1987), and from a sulfide chimney in an active seafloor hydrothermal system (Gena *et al.*, 2013). Both studies attributed the Sn to solid solution. Huston *et al.* (1995) measured up to 2940 ppm Sn in chalcopyrite from the Dry River South VHMS deposit, Eastern Australia, and inferred that Sn substitutes for Fe. They noted that the highest Sn concentrations occur in the more reduced and highly metamorphosed deposits, which is a reflection of the tendency of Sn to only be transported in significant quantities at reduced, high-temperature conditions (Eugster, 1986). George *et al.* (2016) confirmed that in deposits that have recrystallized at amphibolite facies and above, chalcopyrite will typically host more Sn than co-crystallizing sphalerite or galena.

Reports of high levels of manganese in chalcopyrite originate from VMS deposits. Revan *et al.* (2014) reported chalcopyrite containing up to 958 ppm Mn from VMS deposits of the eastern Pontide orogenic belt, NE Turkey, while Maslennikov *et al.* (2009) measured up to 771 ppm Mn in chalcopyrite from the Yaman-Kasy VMS deposit, Southern Urals, Russia.

Chalcopyrite is isostructural with roquesite ($CuInS_2$) and thus significant concentrations of indium can be hosted in chalcopyrite, most probably in the Fe site (Wittmann, 1974). In the SW England ore region, chalcopyrite accounts for the majority of the In budget (locally containing up to 2200 ppm) despite sphalerite and stannite-group minerals typically hosting higher concentrations (Andersen *et al.*, 2016). Cabri *et al.* (1985) reported chalcopyrite from the Kidd Creek deposit, Canada, carrying as much as 1119 ppm In, while Kieft and Damman (1990) measured up to 0.9 wt.% In in chalcopyrite from the Gåsborn area, West Bergslagen, Sweden.

Reports of gallium, mercury and thallium in chalcopyrite are rare and concentrations are almost exclusively in the order of a few ppm (e.g. Maslennikov *et al.*, 2009; McClenaghan *et al.*, 2009; Cook *et al.*, 2011). Revan *et al.* (2014) did, however, report chalcopyrite containing up to hundreds of ppm Tl.

Sample suite

Fifty-three samples were analysed from 15 different deposits in Australia, Bulgaria, Norway, Romania, Serbia and Uzbekistan (Table 2). The selected deposits are from a variety of different ore types including epithermal, skarn, porphyry, VMS, and sedimentary exhalative (SEDEX) systems. Some VMS and SEDEX sulfide ores have been recrystallized due to regional metamorphism and deformation.

Seven samples originated from the Romanian epithermal systems Herja and Toroiaga; and an additional sample was added from the Kochbulak epithermal deposit in Uzbekistan. Six samples originated from the Romanian skarn deposits, Baita Bihor and Oravita. The Bulgarian porphyry deposits of Assarel and Elatsite contributed five samples, and another porphyry sample was from Bor (Serbia). The undeformed Vorta VMS deposit, Romania, and SEDEX Kapp Mineral prospect, Norway, contributed one sample each. SEDEX deposits in which the sulfide assemblages recrystallized during regional metamorphism and deformation (recrystallized SEDEX) contributed eight samples; two from Broken Hill, Australia, and six from Bleikvassli and Mofjell in Norway. Twelve samples came from the Norwegian VMS deposit Sulitjelma, in which the sulfide assemblages also recrystallized during metamorphism and deformation (recrystallized VMS). Finally, eleven samples were added from the Kanmantoo deposit, South Australia, interpreted as a metamorphosed, remobilized syngenetic sulfide ore. Brief descriptions of these deposits are provided as Supplementary Appendix A, together with key references for each.

Experimental methods

Each sample was prepared as a polished block and characterized by reflected light microscopy and back-scattered electron (BSE) imaging prior to LA-ICP-MS analysis. Only areas of chalcopyrite grains free of noticeable inclusions were selected for LA-ICP-MS analysis.

Laser-ablation ICP-MS analysis was carried out using a Resonetics M-50-LR 193 nm Excimer laser attached to an Agilent 7700cx Quadrupole ICP mass spectrometer (Adelaide Microscopy, The University of Adelaide). The Resonetics laser,

https://doi.org/10.1180/minmag.2017.081.021 Published online by Cambridge University Press

TABLE 2. Summary of deposits and samples used in this study.

Deposit/Type	Samples	Conditions of formation or metamorphism	References
Herja, Romania / Epithermal (Neogene)	Hj13	Formed at ~<200°C	Lang (1979); Cook and Damian (1997)
Toroiaga, Romania / Epithermal (Neogene)	Emeric2, T1a, TOR189, TOR191, TOR197, Toroiaga R0	Formed at ~350°C	Szöke and Steclaci (1962); Gotz *et al.* (1990)
Kochbulak, Uzbekistan / Epithermal (Late Paleozoic)	33	Formed at 200–400°C	Kovalenker *et al.* (1997); Islamov *et al.* (1999); Plotinskaya *et al.* (2006)
Baita Bihor, Romania / Skarn Antoniu orepipe – proximal, Marta orepipe – distal (Cretaceous)	BB55 (Antoniu) BBH15-21 (Antoniu)	Formed at ~500°C (proximal), ~375°C (distal)	Cioflica *et al.* (1971, 1977); Shimizu *et al.* (1995); Ciobanu *et al.* (2002)
Oravita, Romania / Skarn (Cretaceous)	ORV1, ORV4, ORV4a, ORV4B		Gheorghițescu (1975); Cioflica and Vlad (1981); Constantinescu *et al.* (1988)
Assarel, Bulgaria / Porphyry (Cretaceous)	ASR 5A, ASR 10, ASR KB P12077	Base metal sulfides formed at 300–150°C	Strashimirov (1993); Popov *et al.* (2000); Strashimirov *et al.* (2002)
Bor, Serbia / Porphyry (Cretaceous)	BOR14	–	Janković (1990); Janković *et al.* (1998)
Elatsite, Bulgaria / Porphyry (Cretaceous)	Elatsite b a, ELS 157	Various assemblages deposited at 190–575°C	Dragov and Petrunov (1996); Georgiev (2008)
Vorta, Romania / VMS (Jurassic)	DMV 99-22	Formed at 250–300°C	Ciobanu *et al.* (2001)
Kapp Mineral, Norway / SEDEX (Late Precambrian?)	Kmi 2a	Very weakly metamorphosed	Flood (1967)
Broken Hill, Australia / Recrystallized SEDEX (Proterozoic)	BH73, BH218	Granulite facies (750–800°C, 5–6 kbar)	Haydon and McConachy (1987); Parr and Plimer (1993); Plimer (2007); Spry *et al.* (2008)
Bleikvassli, Norway / Recrystallized SEDEX (Ordovician)	Bv-1, Bv-4, V598572	Upper amphibolite-lower granulite facies (570°C, 7.5–8 kbar)	Vokes (1963, 1966); Cook *et al.* (1998)
Mofjell, Norway / Recrystallized SEDEX (Paleozoic)	Mo5, Mo16, Mo17A	Amphibolite facies (550°C, 7 kbar?)	Saager (1967); Cook (2001)
Sulitjelma, Norway / Recrystallized VMS (Ordovician)	CV01.1, CV01.2a, CV01.2b, CV01.3, CV01.4, CV01.6b, NC4172, NC5839, NC6894, Su3, Sulis 1b, Sulis2a	Lower amphibolite facies (450–500°C)	Cook *et al.* (1990, 1993); Cook (1992, 1994; 1996); Barrie *et al.* (2010)
Kanmantoo, Australia / Metamorphosed, remobilized syngenetic sulfide ore (Cambrian)	KTDD086(8), KTDD086(9), KTDD086(11), KTDD086(12), KTDD178(7), KTDD178(8), KTDD178(12), KTDD180(3), KTDD180(7), KTDD180S(4), KTDD180S(5)	Amphibolite facies (530–630°C, 2.2–5.4 kbar)	Jensen and Whittle (1969); Verwoerd and Cleghorn (1975); Seccombe *et al.* (1985); Both *et al.* (1995); Spry *et al.* (2010)

Abbreviations: VMS = volcanogenic massive sulfide, SEDEX = sedimentary exhalative.

designed by Laurin Technic Pty., uses a two-volume ablation cell for outstanding trace-element sensitivity, washout and stability (Müller *et al.*, 2009). The ablation cell was filled with UHP He (0.7 L/min) that was mixed with Ar (0.93 L/min) after leaving the cell, and was introduced directly to the torch through a 'squid' (pulse homogenizing device). The ICP-MS was calibrated regularly in order to maximize sensitivity, whilst keeping production of molecular oxide species (i.e. $^{232}Th^{16}O/^{232}Th$) and doubly-charged ion species (i.e. $^{140}Ce^{2+}/^{140}Ce^{+}$) as low as possible, and typically <0.2%.

The laser beam energy output was set at 100 mJ at a 26 μm spot size using a repetition rate of 10 Hz. Each analysis comprised a 30 s background measurement followed by 30 s of sample ablation, while a 40 s delay was allowed after each spot analysis to ensure adequate cell wash-out, gas stabilization, and computer processing time. Analysed isotopes include ^{34}S, ^{55}Mn, ^{57}Fe, ^{59}Co, ^{60}Ni, ^{65}Cu, ^{66}Zn, ^{69}Ga, ^{75}As, ^{82}Se, ^{95}Mo, ^{107}Ag, ^{111}Cd, ^{115}In, ^{118}Sn, ^{121}Sb, ^{125}Te, ^{182}W, ^{197}Au, ^{202}Hg, ^{205}Tl, ^{206}Pb, ^{207}Pb, ^{208}Pb and ^{209}Bi. Dwell times for In, Au and Tl were set to 0.05 s, while all other elements were set to 0.01 s. Mean errors and the minimum detection limits for common trace elements in each sample are provided as Supplementary Appendix B. Typically 10 analyses were made on chalcopyrite in a given sample and as many multiple grains were analysed as possible. Multiple analyses of the MASS-1 sulfide reference material (formerly PS-1; Wilson *et al.*, 2002) bracketed batches of up to 10 unknown analyses. This allowed monitoring of instrument drift, and a linear correction based on the bracketed MASS-1 analyses was applied to all unknown analyses. The latest MASS-1 certificate of analysis (United States Geological Survey, 2014) was used. The stoichiometric nature of chalcopyrite was checked and confirmed by electron probe microanalysis, which also indicated that trace elements were typically present at concentrations below minimum detection limits for that method. Thus, a value of 34.63 wt.% Cu (stoichiometric chalcopyrite) was used as an internal standard. *GLITTER* data reduction software (Van Achterbergh *et al.*, 2001) was used to carry out data calculations. Given poorly constrained sulfur isotopic interference on ^{66}Zn measurements (e.g. Danyushevsky *et al.*, 2011), we accept that the concentration data for Zn reported here may be less accurate than for some other elements. We also acknowledge that there exist a number of other polyatomic interferences that may necessitate, in cases where concentrations of the interfered element are sufficiently high, correction to derive precise abundance data using LA-ICP-MS. Examples include direct mass interference from ^{115}Sn when measuring the content of In (Jenner and O'Neill, 2012), or $^{59}Co^{16}O$ interference when measuring ^{75}As (Patten *et al.*, 2013). We have not made such corrections to the dataset, as, although such interferences can impact on data quality when the elements concerned are present at wt.% concentration = s, we are confident that they are negligible (well within instrumental error) for low ppm values of the order reported here. An exhaustive treatment of all potential interferences for all trace elements would be well beyond the scope of the present manuscript.

Results

Distinguishing whether a trace element is present in solid solution as opposed to microscale mineral inclusions within a given mineral is an ongoing difficulty for microanalytical research (e.g. Cook *et al.*, 2016). In order to produce a reliable dataset, it is integral that all data is properly evaluated and great care is taken to monitor information that may suggest the presence of inclusions (for example LA-ICP-MS downhole spectra; e.g. George *et al.*, 2015, assessing all element combinations that may indicate inclusions; e.g. proton microprobe work of Cabri *et al.*, 1985 or Huston *et al.*, 1995). If not, doubt may be placed on the reliability of any anomalous trace-element report from the literature, especially those where wt.% levels have been measured for trace elements typically present at ppm levels. Nevertheless, one must also be cautious in attributing an anomalous trace-element report from the literature to micro-inclusions of a distinct phase, simply because it is uncharacteristic. Given the right conditions, many minerals may host anomalous concentrations of trace elements not easily attributed to micro-inclusions. We have endeavoured to only analyse areas of chalcopyrite that were free of any noticeable inclusions. Nevertheless, some analyses showed anomalous results, and corresponding LA-ICP-MS downhole spectra revealed irregular profiles implying the presence of micro-inclusions beneath the chalcopyrite surface. Such analyses were discarded. The remaining LA-ICP-MS downhole spectra were relatively smooth indicating measurement of trace-element concentrations in solid solution (Fig. 1). In some cases, where inclusions were

https://doi.org/10.1180/minmag.2017.081.021 Published online by Cambridge University Press

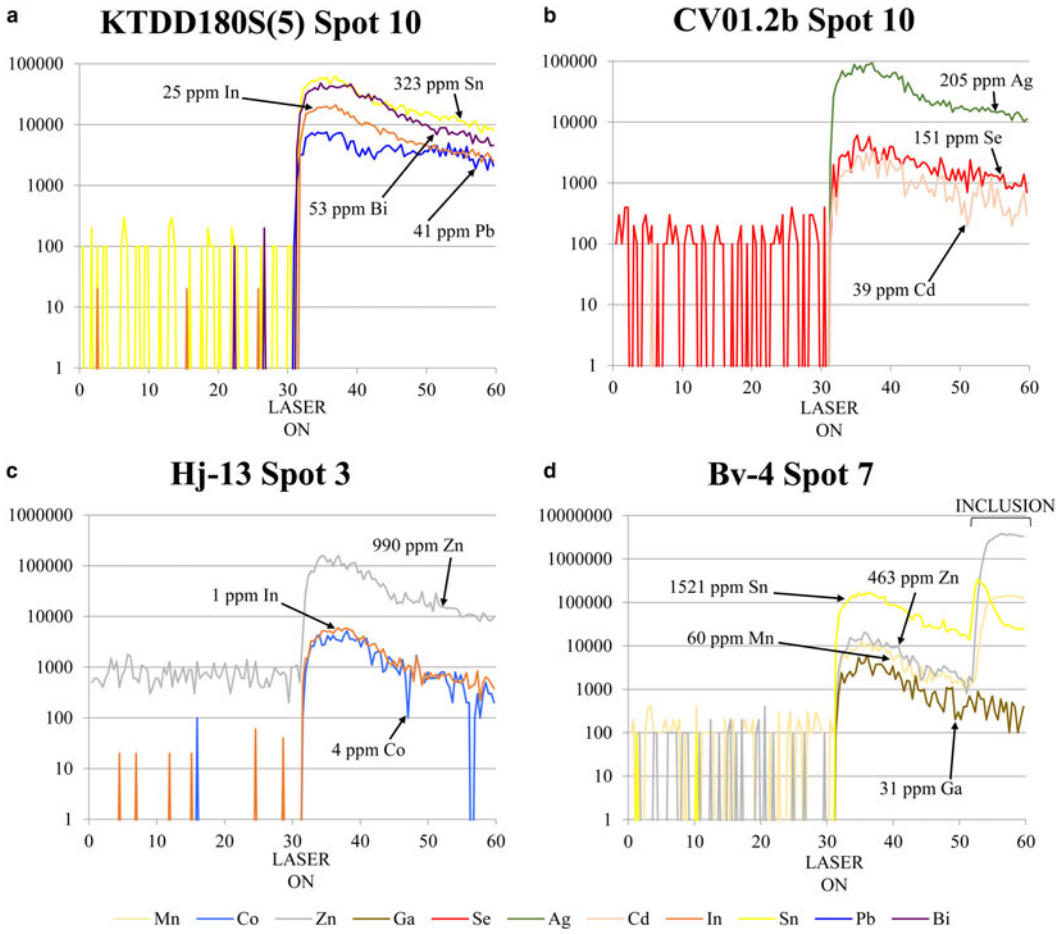

FIG. 1. Representative time-resolved LA-ICP-MS downhole spectra for chalcopyrite. *Y* axis = counts per second, *X* axis = time (s). On each figure the point the laser was fired is indicated on the *X* axis. (*a–c*) Relatively flat spectra reflecting solid solution for Sn, In, Bi, Pb, Ag, Se, Cd, Zn and Co in chalcopyrite from Kanmantoo, Sulitjelma and Herja, respectively. The slight downward trajectory of the spectra indicates a lessening of ablated material over time due to gradual deepening of the ablation hole. (*d*) Relatively flat spectra for Ga (Bleikvassli). Peaks at the end of the Zn, Sn and Mn spectra (as marked on the figure) are suggestive of an inclusion of sphalerite. Concentrations are calculated by selecting and integrating only the signal before the peak.

only present at the end of an individual downhole spectrum (e.g. Fig. 1*d*), concentrations were still calculated by only integrating the signal before the inclusion-related peak. Table 3 summarizes the trace-element data, showing 18 trace elements measured in chalcopyrite. The full dataset is provided as Supplementary Appendix C. Individual spot analyses were plotted as cumulative plots (Fig. 2) allowing visualization of the trace-element variation within each deposit as well as within deposit types. Although the concentrations of some elements in chalcopyrite varied significantly across sample suites from individual deposits, variance was generally limited within any given sample. There was certainly no evidence of systematic grain-scale zonation as has been reported for other base metal sulfides (e.g. galena and sphalerite in low-temperature epithermal ores from Herja; George *et al.*, 2015). Chondrite-normalized distribution plots (Fig. 3) were used to depict the mean trace-element compositions of chalcopyrite (as well as the range of concentrations) in each different deposit

https://doi.org/10.1180/minmag.2017.081.021 Published online by Cambridge University Press

TABLE 3. Summary of trace-element concentrations in chalcopyrite determined by LA-ICP-MS (data in ppm).

Locality	Sample/BMS		Mn	Co	Ni	Zn	Ga	As	Se	Ag	Cd	In	Sn	Sb	Te	Au	Hg	Tl	Pb	Bi
Herja,	Hj-13	M. (10)	51	4.2	0.39	1596	0.09	0.07	8.6	167	7.6	1.7	10	0.71	–	0.001	0.17	0.002	2.0	0.005
Romania	Cp,Sp,Gn	*St. Dev.*	*14*	*1.4*	*0.57*	*699*	*0.05*	*0.04*	*7.7*	*59*	*2.7*	*0.77*	*3.4*	*0.77*	–	*0.001*	*0.04*	*0.002*	*1.6*	*0.003*
Epithermal																				
			Mn	Co	Ni	Zn	Ga	As	Se	Ag	Cd	In	Sn	Sb	Te	Au	Hg	Tl	Pb	Bi
Toroiaga,	EMERIC2	M. (9)	0.2	–	0.06	136	2.0	0.27	19	95	2	32	42	11	–	0.02	1.7	0.003	14	0.22
Romania	Cp,Sp,Gn	*St. Dev.*	–	–	*0.07*	–	*1.4*	*0.31*	*13*	*60*	–	*13*	*25*	*9.3*	–	*0.04*	*2.0*	*0.002*	*15*	*0.30*
Epithermal	T1a	M. (10)	2.4	0.03	–	533	0.60	1.1	1.7	41	10	15	20	2.5	0.25	0.004	0.23	0.001	2.4	0.03
	Cp,Sp,Gn	*St. Dev.*	*2.4*	*0.05*	–	*385*	*0.31*	*0.97*	*1.7*	*38*	*7.8*	*2.4*	*10*	*2.0*	*0.40*	*0.01*	*0.13*	*0.001*	*1.4*	*0.03*
	TOR189	M. (10)	0.98	13	0.28	629	0.27	0.71	78	787	10	20	18	2.2	0.45	0.02	0.46	0.01	1.2	0.9
	Cp	*St. Dev.*	*0.62*	*2.6*	*0.33*	*827*	*0.19*	*0.51*	*27*	*91*	*13.1*	*4.0*	*7.5*	*2.1*	*0.52*	*0.03*	*0.15*	*0.01*	*1.1*	*0.76*
	TOR191	M. (10)	0.8	0.04	0.02	939	0.27	–	1.4	34	19	33	27	0.91	0.02	0.01	234	0.003	1.4	0.01
	Cp,Sp,Gn	*St. Dev.*	*0.97*	*0.05*	*0.02*	*844*	*0.11*	–	*1.8*	*45*	*17.4*	*21*	*16*	*0.63*	*0.02*	*0.02*	*91*	*0.002*	*1.4*	*0.01*
	TOR197	M. (10)	0.9	0.02	0.02	1419	0.12	1.2	1.5	203	25	19	11	1.7	0.10	0.01	292	0.004	3.3	0.02
	Cp,Sp,Gn	*St. Dev.*	*1.4*	*0.05*	*0.03*	*857*	*0.10*	*0.86*	*1.3*	*75*	*16*	*4.7*	*4.1*	*1.6*	*0.10*	*0.01*	*214*	*0.004*	*4.5*	*0.02*
	Toroiaga R0	M. (10)	0.88	0.03	–	1192	0.44	1.6	1.6	5.4	18	18	15	0.56	–	0.002	0.28	–	1.5	0.03
	Cp,Sp,Gn	*St. Dev.*	*1.1*	*0.10*	–	*580*	*0.44*	*1.1*	*1.2*	*7.3*	*7.8*	*7.5*	*12*	*0.35*	–	*0.004*	*0.17*	–	*0.77*	*0.02*
			Mn	Co	Ni	Zn	Ga	As	Se	Ag	Cd	In	Sn	Sb	Te	Au	Hg	Tl	Pb	Bi
Kochbulak,	33	M. (10)	0.88	0.04	0.02	915	0.17	0.86	31	11	19	2.7	11	0.30	0.39	0.02	0.05	0.26	1.5	10
Uzbekistan	Cp	*St. Dev.*	*0.89*	–	*0.07*	*285*	*0.15*	*0.50*	*6.2*	*5.5*	*4.7*	*1.1*	*3.6*	*0.27*	*0.39*	*0.03*	*0.05*	*0.23*	*0.69*	*2.8*
Epithermal																				
			Mn	Co	Ni	Zn	Ga	As	Se	Ag	Cd	In	Sn	Sb	Te	Au	Hg	Tl	Pb	Bi
Baita Bihor,	BB55	M. (10)	6.9	10	0.09	618	0.06	0.32	7.9	14	12	106	122	0.75	0.13	0.12	0.11	0.10	1.7	0.48
Romania	Cp,Gn	*St. Dev.*	*5.5*	*7.6*	*0.10*	*240*	*0.04*	*0.36*	*3.9*	*14*	*13*	*8.8*	*19*	*1.1*	*0.15*	*0.10*	*0.04*	*0.15*	*3.7*	*0.44*
Skarn	BBH15-21	M. (10)	2.1	11	1.3	1041	0.82	0.99	136	35	41	185	176	0.03	1.9	0.03	0.09	0.03	4.6	6.7
	Cp,Sp	*St. Dev.*	*5.3*	*5.8*	*0.91*	*153*	*0.18*	*0.91*	*23*	*7.1*	*10*	*37*	*32*	*0.03*	*1.14*	*0.06*	*0.06*	*0.04*	*2.6*	*3.2*
			Mn	Co	Ni	Zn	Ga	As	Se	Ag	Cd	In	Sn	Sb	Te	Au	Hg	Tl	Pb	Bi
Oravita,	ORV1	M. (10)	0.24	0.15	–	248	0.19	1.4	43	2.9	1.1	8.6	1.1	2.4	0.27	0.01	0.12	0.01	3.3	0.15
Romania	Cp,Gn	*St. Dev.*	*0.19*	*0.10*	–	*120*	*0.12*	*1.0*	*14*	*1.3*	*0.96*	*2.6*	*1.0*	*3.2*	*0.30*	*0.01*	*0.13*	*0.01*	*4.6*	*0.12*
Skarn	ORV4	M. (10)	0.27	0.04	–	156	0.37	2.6	4.7	2.9	1.3	8.1	2.5	1.8	0.08	0.003	0.08	0.01	2.9	0.07
	Cp	*St. Dev.*	*0.17*	*0.05*	–	*26*	*0.43*	*1.6*	*5.5*	*2.5*	*0.71*	*1.6*	*1.5*	*2.6*	*0.17*	*0.01*	*0.08*	*0.01*	*3.9*	*0.08*
	ORV4a	M. (10)	0.17	0.01	0.03	140	0.23	1.0	10	8.0	1.3	9.2	2.0	10	0.22	0.01	0.12	0.05	4.0	0.35
	Cp	*St. Dev.*	*0.11*	*0.02*	*0.09*	*29*	*0.14*	*0.81*	*10*	*4.4*	*1.1*	*1.2*	*1.1*	*21*	*0.31*	*0.01*	*0.07*	*0.09*	*5.5*	*0.97*
	ORV4B	M. (10)	0.10	0.01	0.03	12	0.28	0.40	13	1.3	1.1	0.81	0.43	0.38	0.45	0.03	21	0.09	31	4.7
	Cp,Sp,Gn	*St. Dev.*	*0.07*	*0.03*	*0.03*	*15*	*0.12*	*0.28*	*18*	*1.8*	*1.0*	*0.89*	*0.26*	*0.33*	*0.31*	*0.02*	*14*	*0.20*	*31*	*2.8*
			Mn	Co	Ni	Zn	Ga	As	Se	Ag	Cd	In	Sn	Sb	Te	Au	Hg	Tl	Pb	Bi
Assarel,	ASR 5A	M. (10)	0.53	0.01	–	24	0.52	0.50	12	2.7	2.6	0.20	0.18	0.45	0.27	0.01	35	0.01	8	3.1
Bulgaria	Cp,Sp,Gn	*St. Dev.*	*0.73*	*0.01*	–	*29*	*0.32*	*0.11*	*6.8*	*1.8*	*3.5*	*0.23*	*0.14*	*0.57*	*0.18*	*0.01*	*24*	*0.01*	*7.5*	*2.1*
Porphyry	ASR 10	M. (10)	0.24	–	0.04	11	0.51	0.82	18	2.8	0.27	7.0	0.91	0.12	0.11	0.02	0.07	0.01	5.8	1.3

	Cp	*St. Dev.*	*0.27*	–	*0.12*	*3.8*	*0.34*	*0.30*	*21*	*1.6*	*0.26*	*5.1*	*1.0*	*0.22*	*0.19*	*0.01*	*0.05*	*0.03*	*8.5*	*1.5*
	ASR KB P12077	M. (10)	0.36	0.02	–	8.4	0.20	1.5	226	2.1	0.73	2.8	1.0	0.07	0.54	0.02	0.08	0.02	16	20
	Cp	*St. Dev.*	*0.50*	*0.02*	–	*4.5*	*0.14*	*1.3*	*64*	*2.0*	*0.51*	*0.69*	*0.33*	*0.11*	*0.99*	*0.02*	*0.08*	*0.07*	*27*	*17*
			Mn	Co	Ni	Zn	Ga	As	Se	Ag	Cd	In	Sn	Sb	Te	Au	Hg	Tl	Pb	Bi
Bor, Serbia *Porphyry*	BOR14	M. (10)	2.4	0.05	–	65	0.14	1.3	2.4	12	0.77	0.69	16	0.13	0.04	0.06	0.09	0.23	12	6.2
	Cp	*St. Dev.*	*1.7*	*0.06*	–	*32*	*0.14*	*1.1*	*1.7*	*9.0*	*0.98*	*0.21*	*10*	*0.11*	*0.12*	*0.06*	*0.09*	*0.17*	*10*	*3.3*
			Mn	Co	Ni	Zn	Ga	As	Se	Ag	Cd	In	Sn	Sb	Te	Au	Hg	Tl	Pb	Bi
Elastite, Bulgaria *Porphyry*	Elastite b a	M. (10)	0.60	0.82	–	1.2	0.34	0.78	313	2.5	0.11	2.4	2.0	0.99	0.19	0.002	0.06	0.05	10	1.0
	Cp	*St. Dev.*	*1.1*	*0.65*	–	*1.5*	*0.41*	*0.41*	*240*	*2.9*	*0.19*	*0.25*	*1.6*	*0.97*	*0.29*	*0.004*	*0.06*	*0.06*	*10.6*	*1.2*
	ELS 157	M. (6)	0.76	0.04	–	34	0.96	1.7	2.8	14	0.59	0.35	0.12	4.4	0.23	0.03	0.11	0.01	27	0.61
	Cp,Sp,Gn	*St. Dev.*	*0.62*	*0.09*	–	*10*	*0.34*	*2.0*	*0.86*	*8.4*	*0.41*	*0.08*	*0.06*	*4.5*	*0.27*	*0.02*	*0.15*	*0.02*	*26*	*0.67*
			Mn	Co	Ni	Zn	Ga	As	Se	Ag	Cd	In	Sn	Sb	Te	Au	Hg	Tl	Pb	Bi
Vorta, Romania *VMS*	DMV 99-22	M. (8)	0.27	1.5	–	258	1.0	2.8	–	44	1.2	0.10	0.30	2.4	0.02	0.01	0.72	0.07	8	0.29
	Cp,Sp,Gn	*St. Dev.*	*0.29*	*4.1*	–	*235*	*0.66*	*2.3*	–	*28*	*1.2*	*0.27*	*0.31*	*2.1*	*0.05*	*0.02*	*0.81*	*0.07*	*18*	*0.79*
			Mn	Co	Ni	Zn	Ga	As	Se	Ag	Cd	In	Sn	Sb	Te	Au	Hg	Tl	Pb	Bi
Kapp Mineral, Norway *SEDEX*	kmi 2a	M. (9)	14	0.16	0.26	216	0.16	1.0	2.5	174	3.3	1.4	15	30	0.04	0.01	47	0.06	–	0.26
	Cp,Gn	*St. Dev.*	*20*	*0.15*	*0.28*	*140*	*0.04*	*0.78*	*1.6*	*52*	*2.5*	*0.50*	*4.1*	*17*	*0.05*	*0.01*	*39*	*0.03*	–	*0.32*
			Mn	Co	Ni	Zn	Ga	As	Se	Ag	Cd	In	Sn	Sb	Te	Au	Hg	Tl	Pb	Bi
Broken Hill, Australia *Recrystallized SEDEX*	BH73	M. (5)	23	1.7	0.14	519	5.9	–	–	1112	1.8	1.7	307	0.7	0.05	0.01	0.05	0.10	13	0.01
	Cp,Sp,Gn	*St. Dev.*	*25*	*1.4*	*0.13*	*336*	*1.3*	–	–	*259*	*1.7*	*0.24*	*53*	*0.69*	*0.08*	*0.003*	*0.04*	*0.13*	*13.2*	*0.01*
	BH262	M. (10)	2.5	0.44	0.21	460	8.6	1.2	–	138	2.2	1.3	389	0.60	–	0.002	0.09	0.002	2.5	0.004
	Cp,Sp,Gn	*St. Dev.*	*1.4*	*0.57*	*0.44*	*128*	*4.6*	*0.86*	–	*127*	*1.4*	*0.19*	*69*	*0.52*	–	*0.003*	*0.07*	*0.003*	*2.0*	*0.01*
			Mn	Co	Ni	Zn	Ga	As	Se	Ag	Cd	In	Sn	Sb	Te	Au	Hg	Tl	Pb	Bi
Bleikvassli, Norway *Recrystallized SEDEX*	Bv-1	M. (5)	2.1	0.01	0.01	371	24	–	2.3	597	0.85	19	712	7.3	–	0.24	0.41	0.64	4.1	0.03
	Cp,Sp,Gn	*St. Dev.*	*2.1*	*0.02*	*0.01*	*66*	*14*	–	*1.9*	*295*	*0.25*	*3.5*	*571*	*4.2*	–	*0.35*	*0.28*	*0.65*	*3.4*	*0.03*
	Bv-4	M. (10)	34	0.24	0.10	425	22	1.2	3.5	4.3	2.0	36	1108	3.8	–	0.004	0.17	0.04	1.6	0.06
	Cp,Sp,Gn	*St. Dev.*	*11*	*0.35*	*0.25*	*67*	*9.2*	*0.84*	*2.3*	*2.39*	*0.91*	*3.0*	*362*	*2.9*	–	*0.01*	*0.08*	*0.03*	*1.35*	*0.09*
	V598572	M. (9)	46	0.29	1.3	490	1.7	0.39	13	12	5.6	24	1017	1.0	0.14	0.01	0.85	0.03	2.7	0.02
	Cp,Sp,Gn	*St. Dev.*	*18*	*0.61*	*3.0*	*70*	*1.0*	*0.66*	*10*	*4.0*	*2.8*	*3.7*	*188*	*1.5*	*0.20*	*0.004*	*0.37*	*0.06*	*6.7*	*0.02*
			Mn	Co	Ni	Zn	Ga	As	Se	Ag	Cd	In	Sn	Sb	Te	Au	Hg	Tl	Pb	Bi
Mofjell, Norway *Recrystallized SEDEX*	Mo5	M. (10)	5.3	0.01	1.3	565	0.42	–	16	26	3.1	0.87	3.0	1.1	0.60	0.004	0.16	0.12	2.6	0.01
	Cp,Sp,Gn	*St. Dev.*	*3.3*	*0.02*	*0.83*	*145*	*0.17*	–	*5.4*	*1.8*	*0.75*	*0.35*	*1.3*	*1.8*	*0.70*	*0.004*	*0.09*	*0.27*	*1.5*	*0.01*
	Mo16	M. (10)	0.18	0.01	–	589	0.17	7.8	8.8	12	48	0.11	0.76	2.4	0.26	0.02	0.03	0.01	1.4	0.003
	Cp	*St. Dev.*	*0.14*	*0.02*	–	*86*	*0.10*	*4.0*	*2.2*	*1.0*	*18*	*0.06*	*0.19*	*2.7*	*0.29*	*0.02*	*0.03*	*0.01*	*1.1*	*0.003*
	Mo17A	M. (10)	0.12	0.02	0.01	393	0.15	5.2	3.9	32	51	0.30	0.39	58	0.15	0.02	0.10	0.09	37	0.06
	Cp,Gn	*St. Dev.*	*0.18*	*0.03*	*0.03*	*101*	*0.14*	*3.0*	*2.8*	*22*	*16*	*0.09*	*0.13*	*58*	*0.22*	*0.03*	*0.05*	*0.24*	*37*	*0.10*

(continued)

TABLE 3. (*contd.*)

Locality	Sample/BMS		Mn	Co	Ni	Zn	Ga	As	Se	Ag	Cd	In	Sn	Sb	Te	Au	Hg	Tl	Pb	Bi
Sulitjelma,	CV01.1	M. (10)	0.42	5.8	0.02	699	0.06	1.8	194	248	43	0.46	0.12	–	0.74	0.003	0.16	0.003	0.85	0.22
Norway	Cp	*St. Dev.*	*0.29*	*4.7*	*0.05*	*31*	*0.04*	*1.0*	*14*	*32*	*3.2*	*0.07*	*0.09*	–	*0.64*	*0.003*	*0.09*	*0.002*	*0.54*	*0.15*
Recrystallized	CV01.2a	M. (10)	0.44	7.2	0.09	722	0.10	1.2	166	240	44	0.39	0.08	0.07	1.7	–	0.11	0.002	0.68	0.32
VMS	Cp	*St. Dev.*	*0.24*	*8.3*	*0.14*	*91*	*0.09*	*0.48*	*11*	*89*	*8.9*	*0.04*	*0.04*	*0.07*	*1.1*	–	*0.08*	*0.001*	*0.37*	*0.18*
	CV01.2b	M. (10)	0.27	0.91	–	586	0.04	2.0	153	163	34	0.59	0.09	0.06	1.4	0.002	0.14	0.002	1.1	0.43
	Cp	*St. Dev.*	*0.19*	*0.44*	–	*73*	*0.05*	*1.2*	*11*	*36*	*4.9*	*0.65*	*0.07*	*0.08*	*0.63*	*0.002*	*0.12*	*0.003*	*1.3*	*0.45*
	CV01.3	M. (10)	0.34	0.15	0.07	350	0.20	1.5	849	162	18	0.96	0.26	0.02	0.10	0.004	0.06	0.05	0.29	0.42
	Cp,Sp	*St. Dev.*	*0.25*	*0.12*	*0.12*	*56*	*0.11*	*0.98*	*51*	*32*	*3.8*	*0.11*	*0.17*	*0.02*	*0.16*	*0.01*	*0.04*	*0.14*	*0.18*	*0.20*
	CV01.4	M. (10)	0.23	2.1	0.09	555	0.04	1.0	212	202	27	1.3	0.55	0.14	0.03	0.003	0.22	0.03	0.89	0.62
	Cp	*St. Dev.*	*0.17*	*1.1*	*0.13*	*63*	*0.04*	*0.60*	*11*	*17*	*4.8*	*0.16*	*0.25*	*0.16*	*0.10*	*0.005*	*0.17*	*0.05*	*0.57*	*0.37*
	CV01.6b	M. (10)	0.26	0.19	0.24	394	0.14	1.0	722	196	22	0.67	0.31	0.04	0.08	0.003	0.11	0.01	0.76	0.81
	Cp,Sp	*St. Dev.*	*0.12*	*0.10*	*0.19*	*57*	*0.10*	*0.81*	*42*	*17*	*7.1*	*0.06*	*0.24*	*0.05*	*0.13*	*0.005*	*0.09*	*0.03*	*0.47*	*0.56*
	NC4172	M. (10)	6.0	3.4	0.65	282	0.63	0.97	22	41	4.0	5.4	10	10	0.60	0.01	0.10	0.85	17	4.5
	Cp	*St. Dev.*	*3.3*	*2.0*	*0.78*	*110*	*0.74*	*0.71*	*6.3*	*17*	*1.5*	*1.8*	*1.6*	*3.2*	*0.68*	*0.01*	*0.06*	*0.93*	*10.0*	*2.8*
	NC5839	M. (10)	–	1.1	0.18	471	12	0.94	46	38	2.8	6.3	66	1.5	1.1	0.02	0.13	0.01	1.4	0.25
	Cp,Sp	*St. Dev.*	–	*0.67*	*0.15*	*156*	*3.2*	*0.77*	*8.5*	*5.7*	*1.6*	*1.1*	*6.2*	*1.0*	*0.90*	*0.02*	*0.12*	*0.01*	*0.83*	*0.34*
	NC6894	M. (10)	0.24	0.02	0.02	128	0.37	2.9	68	8.4	2.1	20	53	0.13	1.2	0.05	0.39	0.002	0.46	0.07
	Cp,Sp	*St. Dev.*	*0.20*	*0.04*	*0.03*	*10*	*0.12*	*1.9*	*9.4*	*2.4*	*0.59*	*2.6*	*6.6*	*0.09*	*0.75*	*0.04*	*0.26*	*0.001*	*0.34*	*0.06*
	Su3	M. (10)	0.58	2.4	3.1	148	0.39	0.91	8.7	31	3.3	14	22	0.07	0.70	0.24	0.15	0.001	2.5	5.9
	Cp	*St. Dev.*	*0.83*	*0.60*	*1.3*	*59*	*0.14*	*0.53*	*3.3*	*12*	*0.75*	*0.64*	*7.8*	*0.08*	*0.26*	*0.23*	*0.09*	*0.001*	*2.3*	*2.6*
	Sulis 1b	M. (10)	5.3	0.25	0.11	439	9.0	1.3	53	37	2.8	6.5	58	1.7	0.72	0.01	0.32	0.01	1.3	0.74
	Cp,Sp	*St. Dev.*	*2.8*	*0.27*	*0.27*	*67*	*1.9*	*1.2*	*7.1*	*5.1*	*1.0*	*0.70*	*7.6*	*1.08*	*0.53*	*0.02*	*0.12*	*0.03*	*1.00*	*1.6*
	Sulis2a	M. (10)	16	0.41	0.23	402	2.5	2.0	67	19	5.9	1.5	3.2	1.0	0.85	0.004	0.36	0.001	3.3	0.73
	Cp,Sp	*St. Dev.*	*4.1*	*0.31*	*0.29*	*68*	*0.63*	*1.3*	*7.5*	*3.3*	*1.1*	*0.25*	*1.0*	*0.31*	*0.72*	*0.004*	*0.22*	*0.001*	*2.3*	*1.1*

			Mn	Co	Ni	Zn	Ga	As	Se	Ag	Cd	In	Sn	Sb	Te	Au	Hg	Tl	Pb	Bi
Kanmantoo,	KTDD086(8)	M. (10)	1.3	0.54	1.3	350	2.4	1.1	106	83	1.5	16	80	0.18	0.14	0.12	0.07	0.01	21	2.2
Australia	Cp	*St. Dev.*	*0.39*	*0.43*	*1.04*	*145*	*0.30*	*0.81*	*11*	*115*	*0.75*	*5.4*	*13*	*0.09*	*0.16*	*0.13*	*0.05*	*0.01*	*14*	*1.03*
Metamorphosed	KTDD086(9)	M. (10)	0.68	0.34	0.18	427	2.2	1.4	234	19	1.5	13	58	0.22	0.12	0.07	0.09	0.003	43	2.7
remobilized	Cp	*St. Dev.*	*0.40*	*0.12*	*0.17*	*75*	*1.3*	*0.79*	*64*	*6.6*	*0.33*	*3.4*	*10*	*0.18*	*0.09*	*0.05*	*0.07*	*0.003*	*23*	*1.4*
syngenetic	KTDD086(11)	M. (10)	0.54	0.40	0.14	352	4.3	0.80	48	15	2.0	10	72	0.11	0.60	0.02	0.08	0.003	6.3	0.38
sulfide ore	Cp	*St. Dev.*	*0.25*	*0.12*	*0.14*	*64*	*0.65*	*0.55*	*5.8*	*6.2*	*0.57*	*2.5*	*15*	*0.11*	*0.73*	*0.02*	*0.07*	*0.003*	*2.4*	*0.15*
	KTDD086(12)	M. (10)	0.84	0.35	0.13	390	4.7	1.9	52	20	3.0	15	62	0.14	1.9	0.02	0.11	0.001	5.4	1.3
	Cp	*St. Dev.*	*0.55*	*0.10*	*0.17*	*71*	*1.2*	*1.7*	*5.9*	*9.2*	*0.36*	*3.5*	*11*	*0.09*	*0.76*	*0.02*	*0.12*	*0.001*	*2.0*	*1.2*
	KTDD178(7)	M. (10)	0.13	3.0	0.36	433	0.35	1.0	59	23	1.3	51	149	0.08	0.35	0.02	0.07	0.004	41	1.7
	Cp	*St. Dev.*	*0.09*	*1.1*	*0.21*	*65*	*0.13*	*1.1*	*5.9*	*3.8*	*0.66*	*11*	*64*	*0.06*	*0.22*	*0.02*	*0.06*	*0.003*	*30*	*0.76*
	KTDD178(8)	M. (9)	0.08	0.76	0.57	301	0.46	1.1	50	26	2.3	15	318	–	0.57	0.01	0.06	0.001	1.9	0.10
	Cp	*St. Dev.*	*0.05*	*0.57*	*0.63*	*112*	*0.20*	*1.1*	*18.9*	*11.7*	*0.98*	*6.8*	*142*	–	*0.35*	*0.004*	*0.05*	*0.001*	*1.04*	*0.06*
	KTDD178(12)	M. (10)	0.11	1.3	0.39	356	0.71	0.93	32	43	1.8	19	314	0.03	0.32	0.03	0.07	0.001	1.9	0.21
	Cp	*St. Dev.*	*0.07*	*0.58*	*0.29*	*60*	*0.28*	*0.42*	*3.2*	*8.3*	*0.57*	*9.0*	*100*	*0.01*	*0.27*	*0.02*	*0.05*	*0.001*	*1.3*	*0.14*
	KTDD180(3)	M. (7)	0.80	4.4	0.17	350	0.23	1.6	18	26	0.82	55	24	0.20	0.53	0.003	0.14	0.24	0.92	1.4
	Cp	*St. Dev.*	*0.38*	*4.2*	*0.32*	*63*	*0.13*	*1.3*	*2.5*	*30*	*0.31*	*2.5*	*4.4*	*0.13*	*0.34*	*0.003*	*0.09*	*0.46*	*0.73*	*1.2*
	KTDD180(7)	M. (10)	0.33	0.88	0.42	507	1.4	1.3	12	18	1.3	38	206	0.08	0.88	0.16	0.11	0.17	0.74	3.5
	Cp	*St. Dev.*	*0.22*	*0.35*	*0.39*	*84*	*0.38*	*1.3*	*3.5*	*6.2*	*0.43*	*11*	*47*	*0.05*	*0.58*	*0.14*	*0.07*	*0.54*	*1.2*	*2.8*
	KTDD180S(4)	M. (10)	0.44	2.1	0.06	520	0.59	2.0	54	86	2.3	49	298	0.09	0.37	0.07	0.17	0.01	44	16
	Cp	*St. Dev.*	*0.47*	*1.18*	*0.08*	*63*	*0.13*	*1.5*	*4.5*	*13*	*0.43*	*2.5*	*141*	*0.08*	*0.31*	*0.05*	*0.08*	*0.01*	*14*	*23*

KTDD180S(5)	M. (10)	1.9	2	0.29	389	0.64	1.2	60	123	1.1	21	305	0.16	0.68	0.19	0.11	0.003	28	30
Cp	*St. Dev.*	*1.4*	*3*	*0.39*	*155*	*0.19*	*0.94*	*9.1*	*10*	*0.64*	*3.7*	*82*	*0.11*	*0.58*	*0.09*	*0.09*	*0.002*	*24*	*20*

Abbreviations – BMS: base metal sulfides, Cp: chalcopyrite, Sp: sphalerite, Gn: galena, M.: mean, St. Dev.: standard deviation.
(X) = number of individual spot analyses in that sample. Dash = insufficient data to perform calculation (all analyses < mdl). Other < mdl values were treated as mdl/2.
The 18 elements displayed are commonly present at measurable concentrations. Mo and W were measured but are rarely present above minimum levels of detection.

type. Molybdenum and W were seldom present in chalcopyrite at concentrations above minimum levels of detection (see footnote to Table 3).

Zinc was the trace element most highly concentrated in chalcopyrite – sample Hj-13 from Herja (epithermal) contained chalcopyrite that hosted as much as 1596 ppm Zn. Smooth LA-ICP-MS downhole spectra from Hj-13 indicated the Zn was present in solid solution (Fig. 1*c*). All chalcopyrite in samples from the epithermal deposits contained high levels of Zn; chalcopyrite from porphyry deposits hosted small amounts of Zn. Variation within samples from individual deposits was extremely low, usually only over a single order of magnitude. Chalcopyrite from the epithermal, exhalative and recrystallized exhalative deposit types all had remarkably uniform Zn compositions.

The highest silver concentration in chalcopyrite from any sample analysed here was 1112 ppm (BH73, from the Broken Hill recrystallized SEDEX deposit). High concentrations of Ag appeared typical of chalcopyrite from un-recrystallized and recrystallized exhalative deposits as well as epithermal systems. Chalcopyrite in these deposit types was all similarly enriched in Ag by ~1000 times chondritic concentrations. Chalcopyrite from the skarn at Oravita and the porphyry deposits had the lowest Ag concentrations, usually <10 ppm. Sample variation over one or two orders of magnitude appeared normal within individual deposits (e.g. Toroiaga – epithermal; Baita Bihor – skarn; Mofjell – recrystallized SEDEX etc.).

Tin was highly concentrated in chalcopyrite from the recrystallized SEDEX deposits Broken Hill and Bleikvassli, and also at both Baita Bihor (skarn) and Kanmantoo (metamorphosed, remobilized syngenetic sulfide ore). The most Sn-rich chalcopyrite here was from sample Bv-4 (Bleikvassli; recrystallized SEDEX), which hosted an average of 1108 ppm Sn. Smooth LA-ICP-MS downhole spectra from Bv-4 suggested the Sn was present in solid solution (Fig. 1*d*). Chalcopyrite from Oravita (skarn), Assarel (porphyry), Elatsite (porphyry) and Vorta (VMS) all hosted low levels of Sn. Variation appeared to be considerable within samples from a single deposit, for example, in the case of the Sulitjelma (recrystallized VMS) samples, Sn concentrations in chalcopyrite fluctuated over four orders of magnitude.

The highest concentration of selenium in chalcopyrite here was 849 ppm (from sample CV01.3, Sulitjelma; recrystallized VMS). Sample concentrations varied over three orders of magnitude at

https://doi.org/10.1180/minmag.2017.081.021 Published online by Cambridge University Press

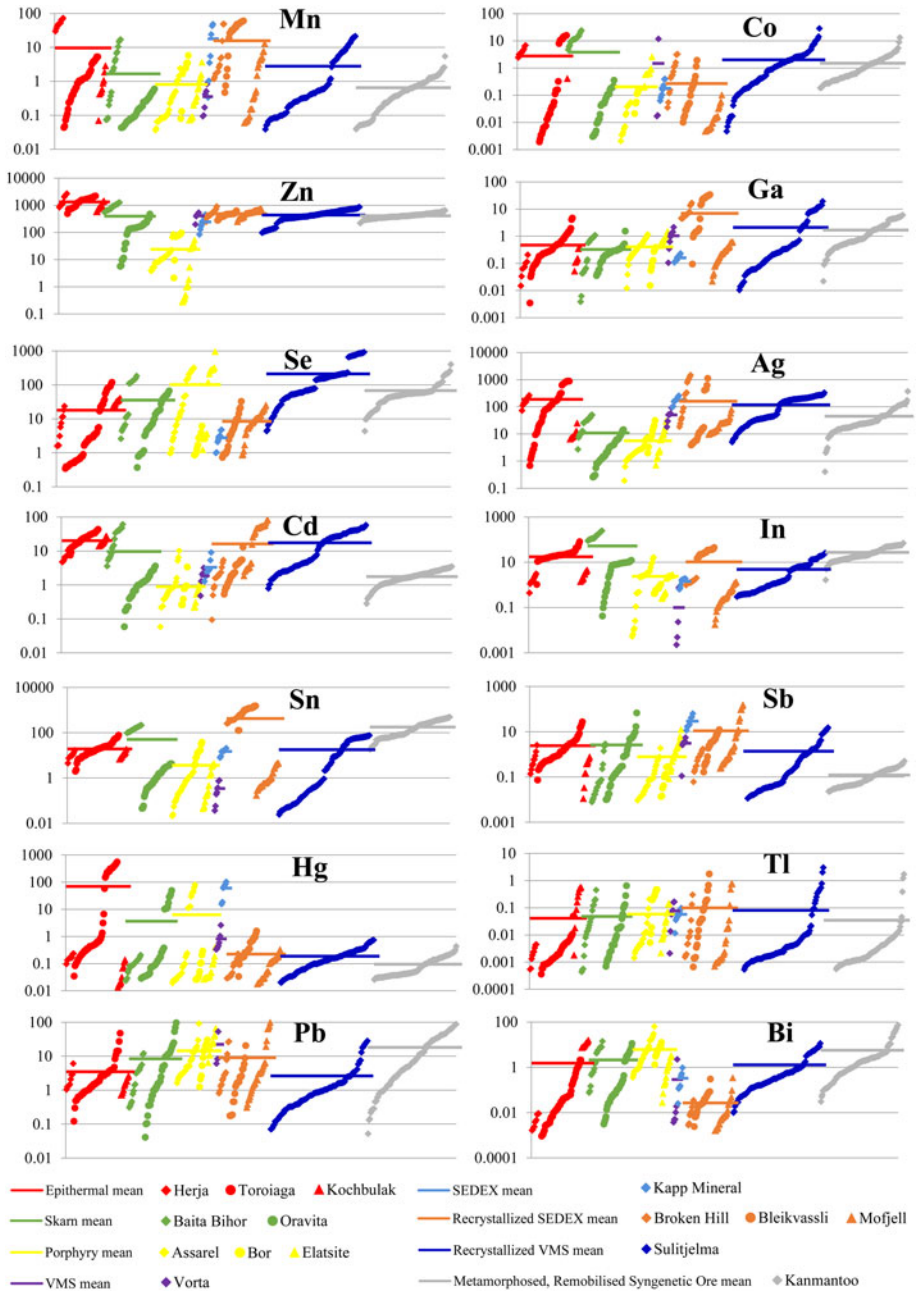

FIG. 2. Cumulative plots showing individual spot concentrations of Mn, Co, Zn, Ga, Se, Ag, Cd, In, Sn, Sb, Hg, Tl, Pb and Bi in chalcopyrite from each deposit. Chalcopyrite concentration data for each deposit is sorted in ascending order and plotted in succession along the *X* axis. *Y* axis = concentration (parts per million). Red points are from epithermal deposits, green are from skarn deposits, yellow are from porphyry deposits, purple are from the Vorta VMS deposit, light blue are from the Kapp Mineral SEDEX prospect, orange are from recrystallized SEDEX deposits, dark blue are from the Sulitjelma recrystallized VMS deposit and grey are from the Kanmantoo deposit, interpreted as a metamorphosed, remobilized syngenetic sulfide ore. The average composition for each deposit type is given as a horizontal coloured line.

https://doi.org/10.1180/minmag.2017.081.021 Published online by Cambridge University Press

Sulitjelma, as well as in the Assarel (porphyry), Elatsite (porphyry) and Toroiaga (epithermal) samples. Typically, however, variation over two orders of magnitude was observed in samples from any deposit. Chalcopyrite from Kapp Mineral (SEDEX) and Bor (porphyry) hosted the least Se. Selenium concentrations in chalcopyrite from exhalative deposits were very uniform, although depleted relative to other deposit types. Overall, mean Se concentrations in chalcopyrite from different deposit types varied by two orders of magnitude.

Chalcopyrite in sample BBH15-21 from Baita Bihor (skarn) hosted 185 ppm In, the most of any sample. Relative to other deposits, In was highly enriched in chalcopyrite at Baita Bihor, as well as Toroiaga (epithermal), Bleikvassli (recrystallized SEDEX) and, to a lesser extent, also at Kanmantoo (metamorphosed, remobilized syngenetic sulfide ore). Indium concentrations in chalcopyrite varied over one or two orders of magnitude within samples from the same deposit, although at Assarel (porphyry), sample concentrations fluctuated over no less than four orders of magnitude. The chalcopyrite in the Vorta (VMS) sample contained the least In. Chalcopyrite from the different deposit types varied in its In content over two orders of magnitude.

We did not record more than 1 ppm mercury and thallium in chalcopyrite across the sample suite, although in a few individual samples chalcopyrite hosted high levels of Hg: samples TOR197 and TOR191 (Toroiaga; epithermal) both contained chalcopyrite hosting over 200 ppm Hg, while tens of ppm were present in chalcopyrite from kmi 2a (Kapp Mineral; SEDEX) and ASR 5A (Assarel; porphyry). Mean Tl concentrations in chalcopyrite from different deposit types varied very little, all approximately uniform with chondritic compositions. Mercury concentrations in chalcopyrite, on the other hand, varied over five orders of magnitude; the most of any element here. Chalcopyrite from recrystallized exhalative deposits was grossly depleted in Hg compared to other deposit types.

Manganese, cadmium and lead were all commonly present in chalcopyrite at concentrations between 0.1 and 50 ppm. Concentrations of Mn and Cd in chalcopyrite samples from any single deposit varied up to two orders of magnitude, although Cd concentrations varied less than that for many deposits. Lead concentrations in chalcopyrite on the other hand fluctuated over three orders of magnitude in samples from a given deposit. The highest mean concentrations in chalcopyrite for each element in any given sample were 51 ppm Mn (V598572; Bleikvassli; recrystallized SEDEX), 51 ppm Cd (Mo17A; Mofjell; recrystallized SEDEX) and 44 ppm Pb (KTDD180S(4); Kanmantoo; metamorphosed, remobilized syngenetic sulfide ore). All epithermal chalcopyrite analysed here was uniformly enriched in Cd relative to other deposit types. While Cd concentrations in recrystallized exhalative chalcopyrite were sometimes also high, the range of concentrations measured was large and extended quite low.

Concentrations of antimony and bismuth in chalcopyrite reached 58 ppm (Mo17A, Mofjell, recrystallized SEDEX) and 30 ppm (KTDD180S (5), Kanmantoo, metamorphosed, remobilized syngenetic sulfide ore), respectively. Concentrations of both elements in chalcopyrite from samples of individual deposits usually varied across two and four orders of magnitude. Kochbulak (epithermal), Baita Bihor (skarn), Assarel (porphyry) and Kanmantoo (metamorphosed, remobilized syngenetic sulfide ore) all hosted chalcopyrite containing high levels of Bi but low levels of Sb, whereas Mofjell (recrystallized SEDEX) chalcopyrite contained high levels of Sb but low levels of Bi. Overall, Sb was most enriched in chalcopyrite from exhalative deposits compared to other deposit types.

Concentrations of cobalt and gallium in chalcopyrite across the sample suite were typically between 0.001 and 10 ppm. Relative to other deposit types, chalcopyrite from the recrystallized exhalative deposits was enriched in Ga, specifically, Bleikvassli (recrystallized SEDEX) and Broken Hill (recrystallized SEDEX). Chalcopyrite concentrations in sample Bv-1 (Bleikvassli) reached 24 ppm Ga. Cobalt concentrations in chalcopyrite were highest in sample TOR189 (Toroiaga; epithermal) where 13 ppm Co was measured. Porphyry chalcopyrite was depleted in Co relative to other deposit types.

Arsenic, nickel, tellurium and gold were all sometimes present at measurable concentrations in chalcopyrite, however individual analyses were frequently below the minimum limit of detection. The highest concentrations of these elements in chalcopyrite was 7.8 ppm As (Mo16; Mofjell; recrystallized SEDEX), 3.1 ppm Ni (Su3; Sulitjelma; recrystallized VMS), 1.9 ppm Te (in both BBH15-21; Baita Bihor; epithermal, and KTDD086(12); Kanmantoo; metamorphosed, remobilized syngenetic sulfide ore) and 0.24 ppm Au (in both Bv-1; Bleikvassli; recrystallized SEDEX, and Su3; Sulitjelma; recrystallized VMS).

https://doi.org/10.1180/minmag.2017.081.021 Published online by Cambridge University Press

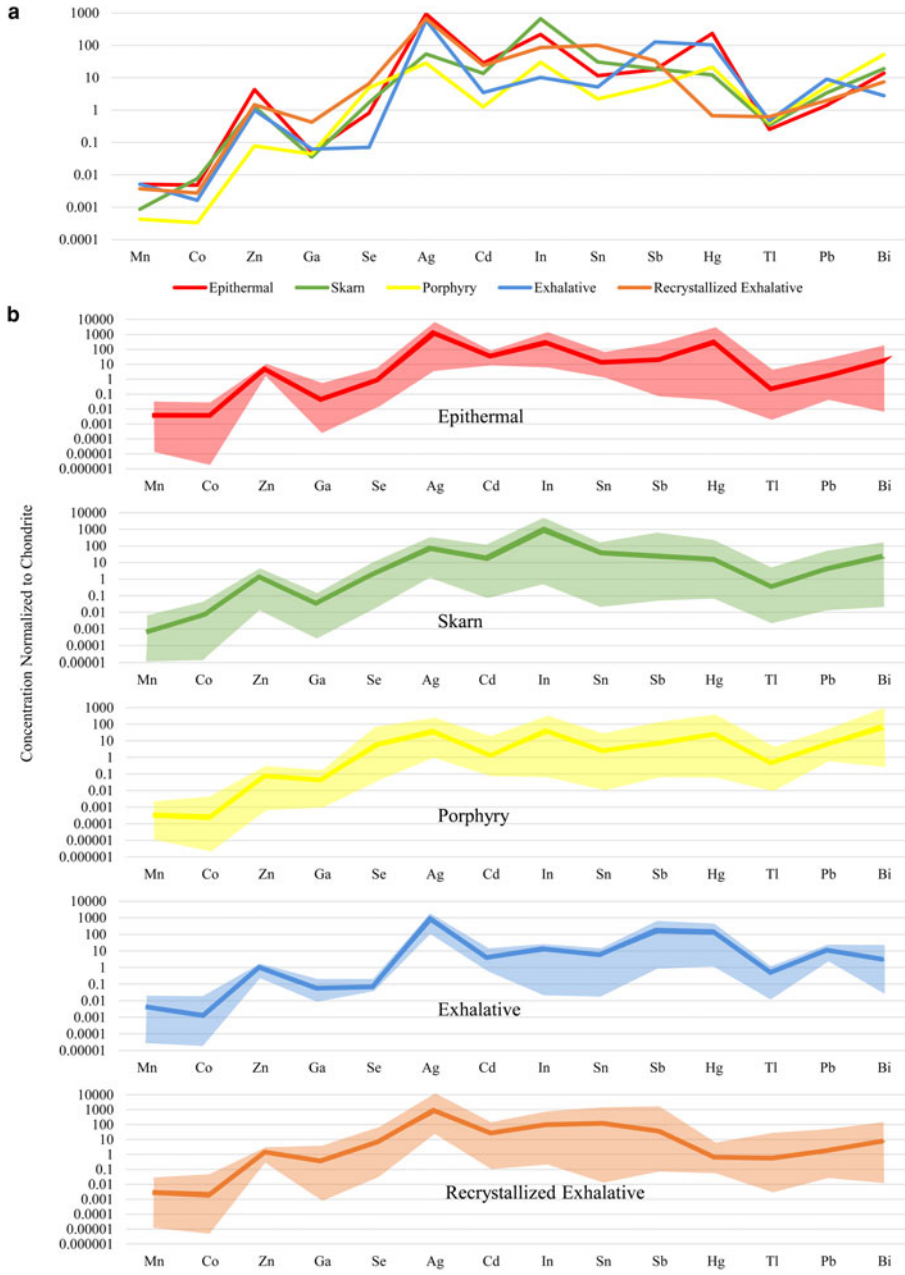

FIG. 3. Chondrite-normalized distribution plots for 14 common trace elements in chalcopyrite from different deposit types. Data normalized with values from McDonough and Sun (1995). (*a*) Comparison of the mean concentration of each trace element in chalcopyrite from different deposit types. (*b*) Mean concentration and range of each trace element in chalcopyrite from epithermal, skarn, porphyry, exhalative and recrystallized exhalative deposits. Epithermal deposits consist of Herja, Toroiaga and Kochbulak, skarn deposits consist of Baita Bihor and Oravita, Porphyry deposits consist of Assarel, Bor and Elatsite, exhalative deposits consist of Vorta and Kapp Mineral and recrystallized exhalative deposits consist of Broken Hill, Bleikvassli, Mofjell and Sulitjelma.

https://doi.org/10.1180/minmag.2017.081.021 Published online by Cambridge University Press

Discussion

Chalcopyrite as a trace-element host

Chalcopyrite is generally considered to be a relatively poor host for trace elements, at least if compared to other common Cu-(Fe)-sulfides (e.g. bornite and chalcocite; Cook *et al.*, 2011), sphalerite (Cook *et al.*, 2009) or galena (George *et al.*, 2015). Indeed, LA-ICP-MS element distribution maps in George *et al.* (2016) demonstrated that chalcopyrite is generally the 'least preferred' host for a range of trace elements when chalcopyrite, sphalerite and galena are inferred to co-crystallize.

A summary of relevant literature reveals that only Ag, Zn, As, Se, Co and Pb are usually reported as trace components in solid solution within chalcopyrite, whereas Mn, In, Tl, Ga and Hg are seldom referred to, if at all. There is also a relative scarcity of empirical concentration data for natural chalcopyrite compared to other sulfides, and in cases where data are reported, often the full range of elements were not checked, or the minimum levels of detection for many trace elements were too high to gain a proper appreciation of concentration ranges (e.g. Harris *et al.*, 1984; Cabri *et al.*, 1985; Kase, 1987; Brill, 1989; Huston *et al.*, 1996; Scott *et al.*, 2001; Moggi-Cecchi *et al.*, 2002; Serranti *et al.*, 2002; Shalaby *et al.*, 2004; Demir *et al.*, 2008; Layton-Matthews *et al.*, 2008; Monteiro *et al.*, 2008; Demir *et al.*, 2013; Gena *et al.*, 2013; Reich *et al.*, 2013; Cioacă *et al.*, 2014; Helmy *et al.*, 2014; Wang *et al.*, 2015*a*; Wohlgemuth-Ueberwasser *et al.*, 2015; Sadati *et al.*, 2016). The dataset presented in this study, encompassing a wider range of trace elements, and with the generally lower minimum detection limits afforded by LA-ICP-MS, thus allow for a new evaluation of chalcopyrite as a trace-element carrier.

Zinc was the most abundant trace element present in the chalcopyrite analysed here with individual spot concentrations exceeding 2000 ppm in the Herja and Toroiaga epithermal systems. The only other trace elements commonly present at >100 ppm were Se, Ag and Sn. As such, the trace-element budget for chalcopyrite was generally lower than in other co-existing base-metal sulfides for which data are available (e.g. Cook *et al.*, 2011; George *et al.*, 2016). Yet regardless of the lower overall concentrations compared to other common sulfides, particularly when they co-crystallize with chalcopyrite, it is apparent that the latter is able to incorporate a wide range of trace elements. Manganese, Co, Zn, Ga, Se, Ag, Cd, In, Sn, Sb, Hg, Tl, Pb and Bi were all commonly present at measurable levels in chalcopyrite. Generally, trace-element concentrations showed little variation at the sample scale, yet most elements showed significant variation of four to five orders of magnitude across the sample suite and even from samples within individual deposits. Significantly, Mn, In, Tl, Ga and Hg were all commonly present at measurable concentrations in chalcopyrite despite rarely being reported in most previous studies. Other trace elements that were occasionally present in chalcopyrite include Ni, As, Te and Au. Thus, considering the greater abundance of chalcopyrite relative to other sulfides in many Cu-ores, in a given deposit chalcopyrite may be the main sulfide host for many of the elements listed above.

Trace-element incorporation

The incorporation of trace elements into the chalcopyrite structure is more complex than in other common base-metal sulfides, particularly sphalerite or galena. Covalent bonding in chalcopyrite means that Goldschmidt's rules (Goldschmidt, 1954) cannot be used to predict partitioning trends as for purely ionic structures (e.g. George *et al.*, 2016). Instead, in any given ore system, the trace-element content of chalcopyrite will depend principally on the presence or absence of other co-crystallizing sulfides, particularly sphalerite and galena. All trace elements analysed here (except for Zn in the absence of sphalerite) preferentially partition into co-crystallizing sphalerite or galena if those phases are present (George *et al.*, 2016). This is demonstrated in Figs 4*a* and *b*, which show the concentration of different trace elements in chalcopyrite from Toroiaga and Oravita, respectively. In the first case, Co, Se, Ag and Bi concentrations are all significantly lower in hydrothermal chalcopyrite that co-crystallized with sphalerite and galena than in chalcopyrite from assemblages in which the other base-metal sulfides are absent (Fig. 4*a*). This supports observations (George *et al.*, 2016) that Co will preferentially partition into sphalerite, and Se, Ag and Bi into galena, when those base-metal sulfides co-crystallize with chalcopyrite in hydrothermal settings. At Oravita, Co, Zn, Ag, In and Sn concentrations are all significantly lower in chalcopyrite associated with sphalerite compared to chalcopyrite that has crystallized without any sphalerite in the polished section (Fig. 4*b*). Again

https://doi.org/10.1180/minmag.2017.081.021 Published online by Cambridge University Press

the sphalerite has incorporated a significant proportion of the trace-element budget. We thus conclude that hydrothermal chalcopyrite crystallizing without sphalerite and/or galena, is likely to host greater concentrations of Co, Zn, Se, Ag, In, Sn and Bi, whereas the concentration of these elements will be reduced when sphalerite and/or galena co-crystallize. Consequently, chalcopyrite may be thought of as a sink that will incorporate much of the 'leftover trace-element budget' not taken up into other co-crystallizing sulfides (sphalerite and galena in the cases above), and explains efficiently why chalcopyrite is able to host a wide range of trace elements while measured concentrations are generally low. A similar relationship exists between chalcopyrite and pyrite, the latter well known to incorporate high levels of As, Co and Ni, and possibly also others (e.g. Large *et al.*, 2009; Winderbaum *et al.*, 2012). Similarly, in ores containing bornite and/or chalcocite, such as Olympic Dam, South Australia, these minerals are likely to host, and control the distribution of Ag and Bi, with chalcopyrite only an important Ag-Bi-host when bornite and chalcocite are absent (Cook *et al.*, 2015).

In the case of those deposits in which the sulfides recrystallized during syn-metamorphic deformation (Broken Hill, Bleikvassli, Mofjell and Sulitjelma), the presence or absence of other co-crystallizing base-metal sulfides influences trace-element incorporation into chalcopyrite in a different way. Under metamorphic conditions of amphibolite facies or above, both Ga and Sn will partition typically into chalcopyrite over co-crystallizing sphalerite, distinct from the preferred host of these trace elements at lower temperatures (sphalerite in the case of Ga; George *et al.*, 2016). This is illustrated by Fig. 4*c*, which shows the concentration of different trace elements in chalcopyrite from recrystallized samples from the Sulitjelma VMS deposit. Concentrations of Co are significantly lower in chalcopyrite that has recrystallized together with sphalerite if compared to chalcopyrite-only assemblages. This is the same trend depicted in Figs 4*a* and *b*, showing that Co is preferentially partitioned into sphalerite over chalcopyrite at all temperatures and pressures (George *et al.*, 2016). The trends for Ga and Sn contrast, however, with those shown by Co, in that the concentrations of both Ga and Sn are significantly higher in chalcopyrite that has recrystallized with sphalerite. Our interpretation is that, during recrystallization associated with sub-solidus deformation, Ga and Sn present in pre-existing sphalerite has been remobilized and re-partitioned into chalcopyrite thus increasing the concentration of these elements in the latter, more so than if it had recrystallized alone.

Other factors certainly also play a contributing role in trace-element incorporation into chalcopyrite. For example, Tl is incorporated preferentially into galena over either chalcopyrite or sphalerite (George *et al.*, 2016). However, in the absence of galena and/or sphalerite, chalcopyrite will still not host more than negligible concentrations of Tl (never more than a few ppm in the sample suite analysed here). There must therefore be factors intrinsic to the chalcopyrite crystal structure that influence trace-element incorporation. Bonding in the chalcopyrite structure is strongly covalent with an effective ionic state between $Cu^{+}Fe^{3+}S_2^{2-}$ and $Cu^{2+}Fe^{2+}S_2^{2-}$ (Li *et al.*, 2013). Yet Goldschmidt's rules for trace-element incorporation into ionic structures (Goldschmidt, 1954) may still be helpful in understanding the observed trace-element trends in chalcopyrite. As per Goldschmidt's rules, the ionic radius of a substituting trace element is a major control on trace-element incorporation. The ionic radii of Zn^{2+}, Sn^{4+} and In^{3+} in tetrahedral coordination all fall within a 'window' between the ionic radii of Fe^{3+} and Fe^{2+} (Fig. 5). Although Ag^{+} is significantly outside this 'window', it is still the monovalent ion closest in size to Cu^{+} in tetrahedral coordination. These elements (plus Se which can be assumed to substitute for S) were the highest concentration trace constituents measured in chalcopyrite here. Ni^{2+} and Co^{2+} also fall within the Fe^{3+} and Fe^{2+} 'window' but were never significantly concentrated in chalcopyrite here, possibly due to their incorporation into nearly ubiquitous pyrite. Occasional studies have, however, measured high concentrations of Co and Ni in chalcopyrite (e.g. Bajwah *et al.*, 1987; Thole, 1976; Wang *et al.*, 2015*a*; Wang *et al.*, 2015*b*). Despite the above observations, mechanisms of trace-element incorporation into covalent structures represents a significant research gap and further study is needed to understand partitioning controls.

Correlation between Cd and Zn

A noteworthy correlation between Cd and Zn concentrations in chalcopyrite is observed across the dataset. This strong correlation is unique as all other trace-element pairs show little to no correlation. In general, higher Zn concentrations in chalcopyrite are associated with higher Cd concentrations. Concentration data from a number of

https://doi.org/10.1180/minmag.2017.081.021 Published online by Cambridge University Press

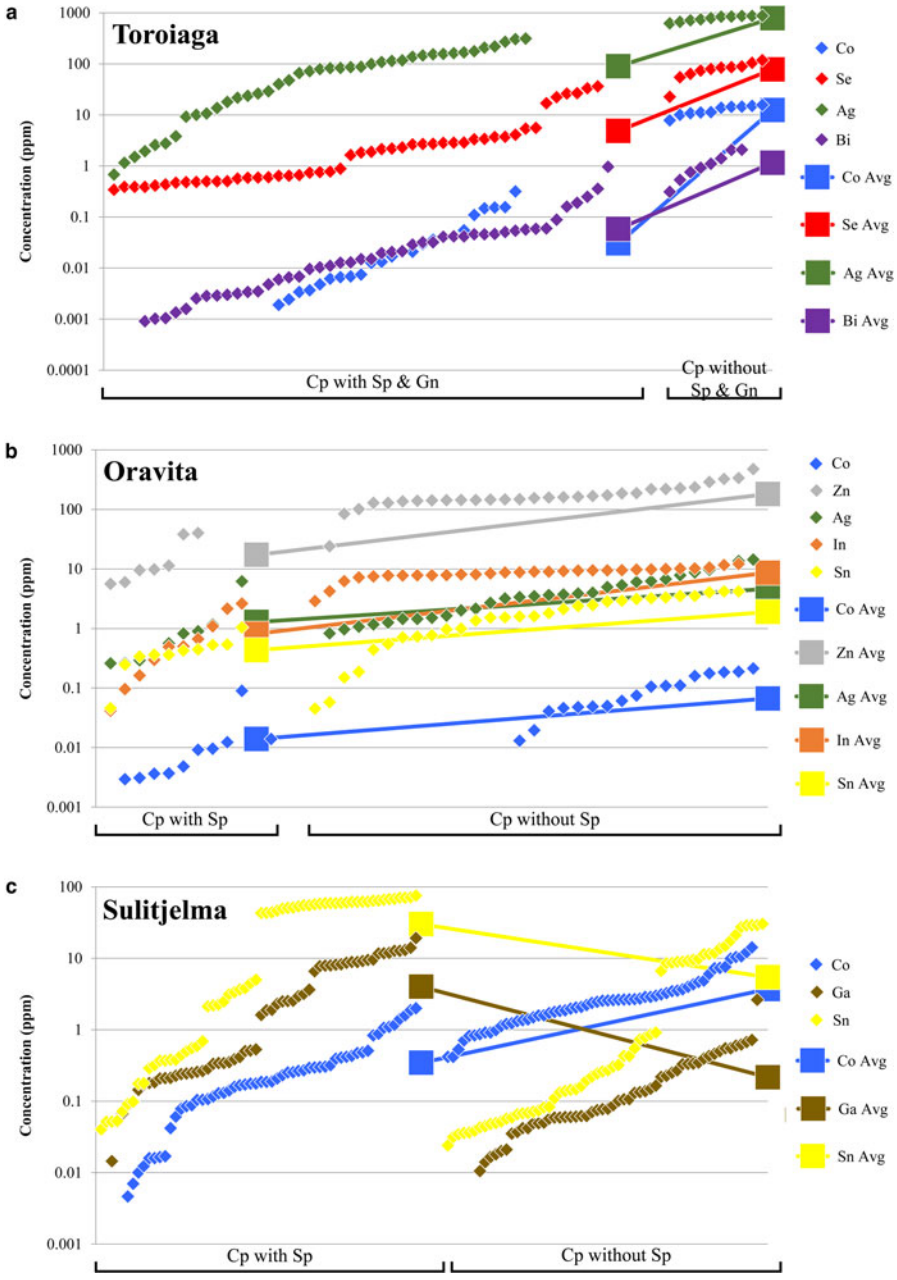

FIG. 4. Plots showing the dependency of the trace-element composition of chalcopyrite on co-crystallizing base-metal sulfides (BMS). Chalcopyrite concentration data for each BMS assemblage in each deposit is sorted in ascending order and plotted in succession along the *X* axis. (*a*) Chalcopyrite in samples from Toroiaga. Data to the left of plot is from chalcopyrite co-crystallizing with sphalerite and galena. Data to the right of plot is from chalcopyrite crystallizing without other BMS nearby. (*b*) Chalcopyrite in samples from Oravita. Data to the left of plot is from chalcopyrite co-crystallizing with sphalerite. Data to the right of plot is from chalcopyrite crystallizing without other BMS nearby. (*c*) Chalcopyrite at Sulitjelma. Data to the left of plot is from chalcopyrite co-crystallizing with sphalerite. Data to the right of plot is from chalcopyrite without other BMS crystallized nearby.

https://doi.org/10.1180/minmag.2017.081.021 Published online by Cambridge University Press

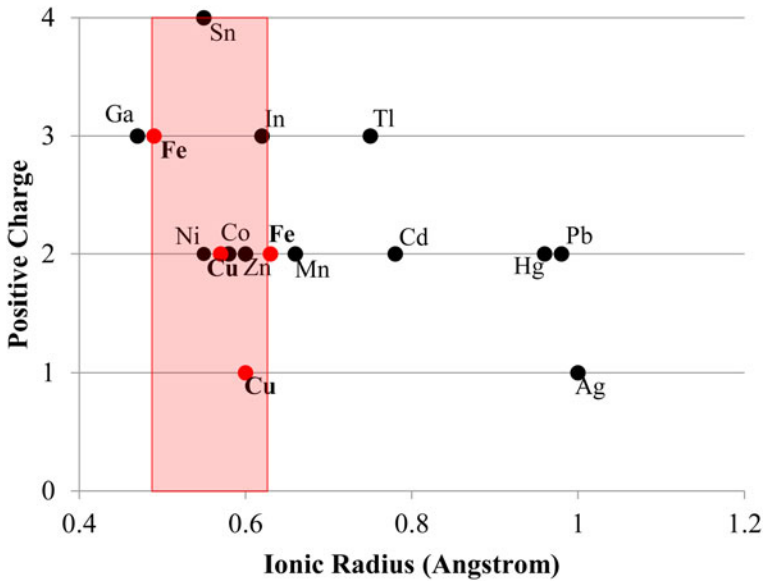

FIG. 5. Plot showing the ionic radius of various trace-element ions in tetrahedral coordination – as in chalcopyrite (data from Shannon, 1976). Red dots represent Fe^{3+}, Cu^{2+}, Cu^{+} and Fe^{2+}. The red area represents the zone in which trace elements have ideal ionic radii for incorporation into chalcopyrite.

individual deposits fit well to lines of differing positive slope that pass through the origin (Fig. 6*a*), such that chalcopyrite from individual deposits display relatively constant Cd:Zn ratios. This ratio increases from the VMS Vorta deposit (0.002), to the Herja epithermal system (0.003), to the SEDEX Kapp Mineral deposit (0.007), to the Toroiaga (0.010) and Kochbulak (0.012) epithermal systems, to the Baita Bihor skarn (0.017) and finally to the recrystallized VMS and SEDEX deposits Sulitjelma (0.021) and Mofjell (0.042), respectively. The Cd:Zn ratio in chalcopyrite (Cd/Zn_{cp}) increases with the inferred temperature of crystallization, thus strongly suggesting that temperature is a significant factor influencing Cd/Zn_{cp}, as illustrated by Fig. 7. We note that this same trend is observed when chalcopyrite data are plotted for samples without any coexisting sphalerite (Fig. 6*b*). The data are thus unlikely to be influenced by sphalerite inclusions accidently (co)-analysed in the chalcopyrite, except perhaps in one population of chalcopyrite from Mofjell with low Cd but relatively high Zn.

Although crystallization temperature clearly influences Cd/Zn_{cp}, it is unlikely to be the sole factor controlling incorporation of the two elements. For instance, the Cd/Zn_{cp} for Broken Hill (0.002) and Bleikvassli (0.004) appear anomalous as they are far too low to solely reflect sulfide crystallization temperature in these high-temperature deposits. Schwartz (2000) noted similar systematic variation in the Cd:Zn ratio of sphalerite (Cd/Zn_{sp}) in different deposit types, particularly among Mississippi Valley-type (MVT) and exhalative (VMS and SEDEX) deposits. Schwartz reasoned that temperature played a role in determining Cd/Zn_{sp} but noted that reduced f_{S_2} and pH were also significant. These three factors control the stability of Cd and Zn complexes in an ore fluid, and thus the partitioning coefficients of Cd and Zn. Regardless, these influences alone cannot explain Cd:Zn ratios in natural sphalerites, prompting Schwartz (2000) to conclude that the Cd:Zn ratio in the ore-forming fluid is the most important factor in determining Cd/Zn_{sp}. A similar conclusion was reached by Gottesmann and Kampe (2007).

It is probable that the Cd:Zn ratio in the ore-forming fluid, as well as factors controlling the stability of Cd and Zn complexes in the fluid (e.g. temperature, sulfur activity, pH), would also control Cd/Zn_{cp}. Thus specific physiochemical conditions should result in a particular Cd:Zn ratio in either sphalerite or chalcopyrite, and this ratio should remain constant if the physiochemical conditions do not change. Consequently, chalcopyrite from an individual deposit that has a relatively constant Cd:Zn ratio probably

https://doi.org/10.1180/minmag.2017.081.021 Published online by Cambridge University Press

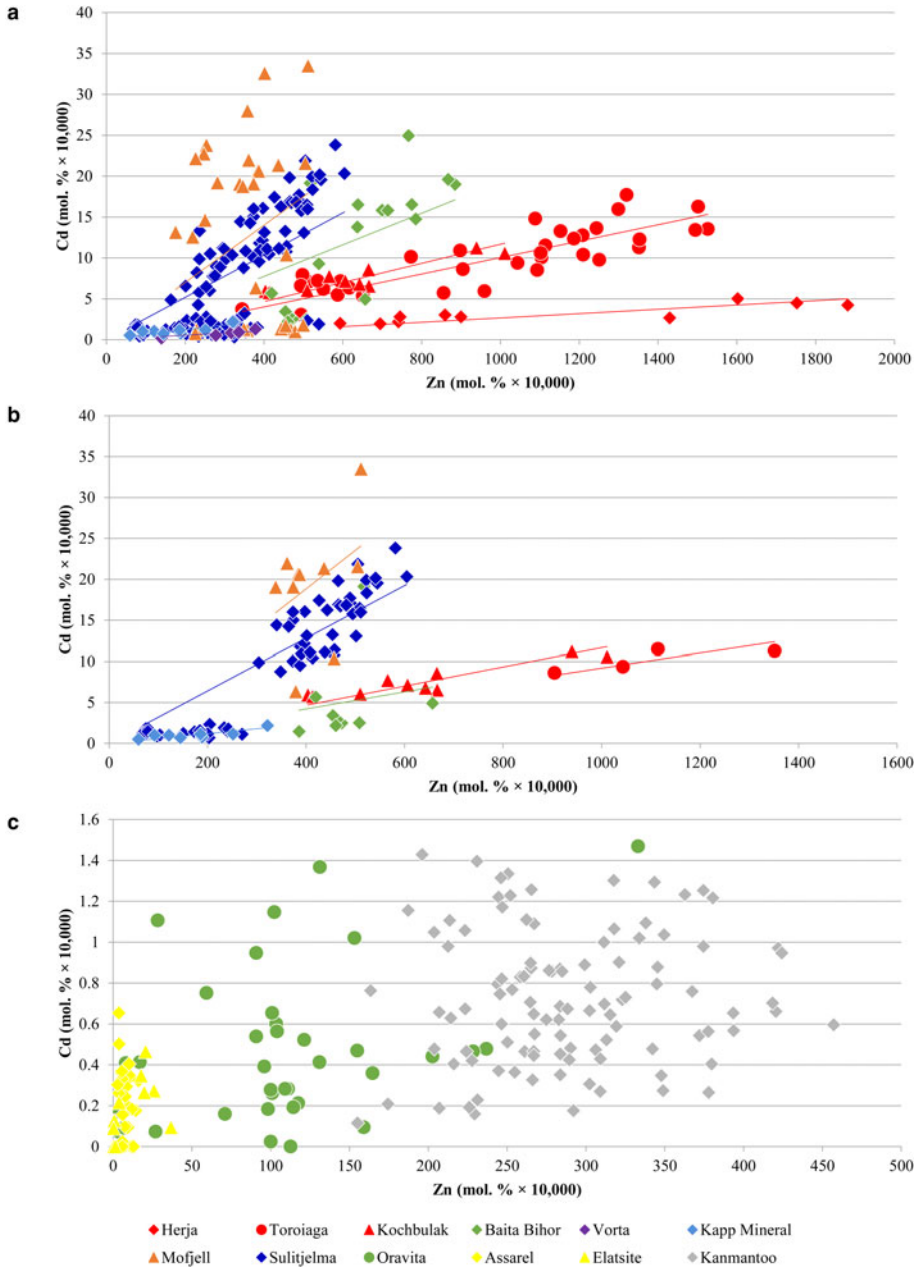

FIG. 6. Binary plots showing the correlation between Cd and Zn in chalcopyrite. (*a*) Data for Herja, Toroiaga, Kochbulak, Baita Bihor, Vorta, Kapp Mineral, Mofjell and Sulitjelma fit well to lines of positive slope that pass through the origin. (*b*) Only data from samples with no coexisting sphalerite are plotted. As general trends remain, the data are unlikely to be influenced by sphalerite inclusions accidently (co)-analysed in the chalcopyrite. (*c*) Data from Oravita, Assarel, Elatsite and Kanmantoo do not fit to lines of positive slope. See text for explanation.

https://doi.org/10.1180/minmag.2017.081.021 Published online by Cambridge University Press

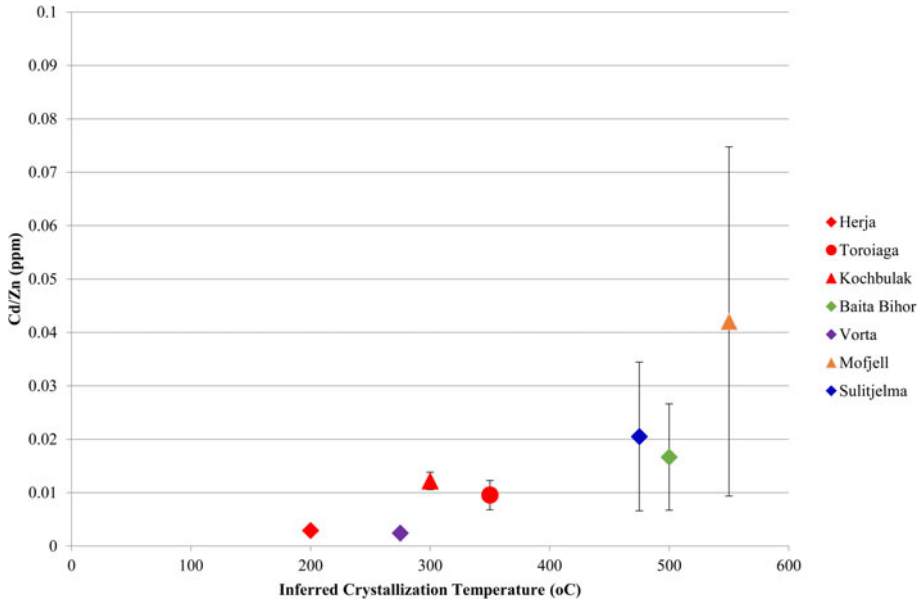

FIG. 7. Plot showing the correlation between the Cd:Zn ratio in chalcopyrite and inferred chalcopyrite crystallization temperature. Inferred crystallization temperatures are only estimates. Deposits with no known crystallization temperatures have not been plotted, nor have those deposits for which chalcopyrite Cd *vs*. Zn plots do not correlate well along a line of positive slope. Error bars represent one standard deviation.

crystallized in a system during which the physiochemical conditions remained constant. In deposits such as Oravita, Assarel, Elatsite and Kanmantoo, where the Cd *vs*. Zn plots for chalcopyrite do not correlate well along a line of positive slope (Fig. 6*c*), chalcopyrite probably crystallized under evolving, and possibly highly localized physiochemical conditions.

The mean Cd:Zn ratios in chalcopyrite and co-crystallizing sphalerite are shown in Fig. 8. In most samples chalcopyrite and sphalerite have very similar Cd:Zn ratios. As the Cd:Zn ratio in the ore-forming fluid is the most important factor in determining Cd/Zn_{sp}, the relationship between chalcopyrite and sphalerite is probably a reflection of co-crystallization from a common ore-forming fluid, in which case the ore fluid Cd:Zn ratio is also the most critical factor in controlling Cd/Zn_{cp}. Nevertheless, some samples do show differences in the Cd:Zn ratios of the two minerals. Typically, when a difference is present, the Cd:Zn ratio is higher in chalcopyrite than in sphalerite. Samples from Oravita, Assarel and Elatsite reveal mean chalcopyrite Cd:Zn ratios that are an order of magnitude greater than in sphalerite. Interestingly, these are the same deposits for which chalcopyrite Cd *vs*. Zn plots do not correlate well, and where changing physiochemical conditions were invoked to explain the observed trends (Fig. 6*c*). It thus seems that evolving physiochemical conditions may affect Cd/Zn_{cp} to a greater extent than Cd/Zn_{sp}, leading to marked differences in the mean Cd:Zn ratios of the two minerals. This is intuitive as Cd and Zn concentrations in chalcopyrite may vary over three and four orders of magnitude, respectively, allowing Cd/Zn_{cp} to change over a possible seven orders of magnitude. In sphalerite, however, Cd concentrations generally vary over only one order of magnitude (Cook *et al.*, 2009), and Zn concentrations are fixed, so limiting the Cd/Zn_{sp} to vary no more than one order of magnitude.

The Cd:Zn ratios in chalcopyrite and sphalerite may be useful in indicating whether physiochemical conditions remained constant during base-metal sulfide crystallization. A fixed Cd/Zn_{cp} approximately equal to Cd/Zn_{sp} would indicate co-crystallization of the two sulfides from the same ore-forming fluid under constant physiochemical conditions. If Cd/Zn_{cp} is constant yet distinct from Cd/Zn_{sp}, the two sulfides probably crystallized at different times and/or from different ore-forming fluids. A non-constant Cd/Zn_{cp}, especially if

https://doi.org/10.1180/minmag.2017.081.021 Published online by Cambridge University Press

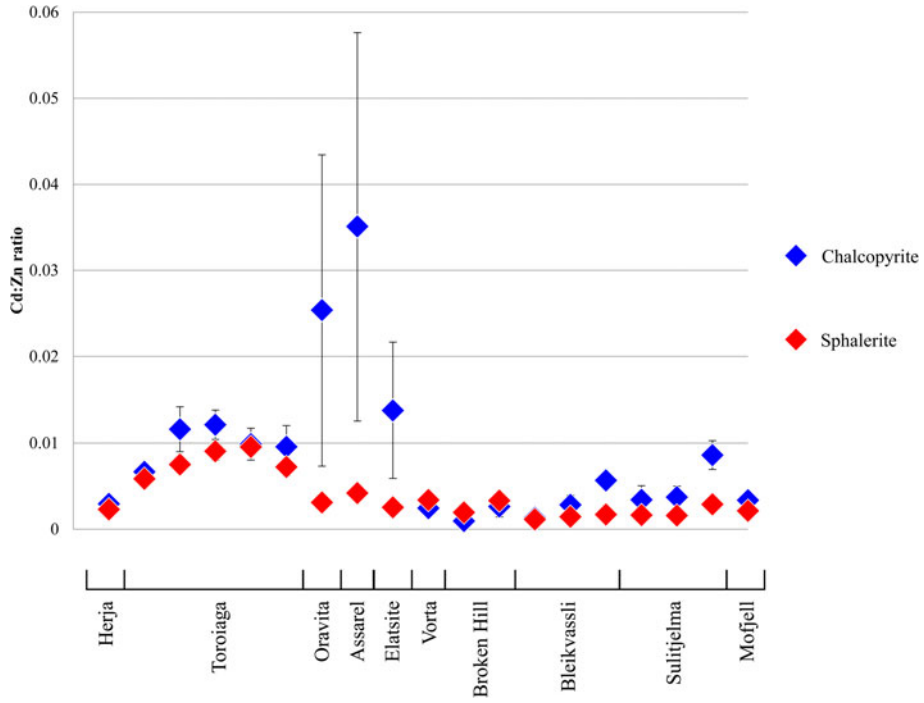

FIG. 8. Plot showing the similarity between the Cd:Zn ratios in chalcopyrite and co-crystallizing sphalerite from various deposits. Error bars represent one standard deviation.

combined with a distinct difference in Cd/Zn_{sp} indicates varying physiochemical conditions during sulfide crystallization. A more thorough investigation is required to determine how Cd/Zn_{cp} depends on ore-forming fluid chemistry and/or other factors. The temperature-dependant nature of the Cd:Zn ratio in both sphalerite and chalcopyrite may even potentially allow a geothermometer to be defined based on the partitioning of Cd and Zn among sphalerite-chalcopyrite pairs, assuming other factors affecting Cd/Zn_{cp} and Cd/Zn_{sp} can be accounted for.

Deleterious elements

Knowledge of, or the ability to predict, the trace-element chemistry of base-metal sulfides carries critical economic implications. The presence of harmful or unwanted elements (deleterious elements) in sulfide copper ores is a significant concern for many mining operations selling their concentrate on the world market. If bound within the lattice of the common Cu-(Fe)-sulfides (chalcopyrite, bornite, chalcocite) or as inclusions within those minerals, elements including Co, Zn, As, Se, Cd, Sb, Hg, Pb and Bi will move to copper concentrates after froth flotation (Mular *et al.*, 2002). Such elements reduce the overall grade of the copper concentrate and may require further, typically costly treatment to remove them from final copper products. Smelters thus impose financial penalties on concentrates which contain deleterious elements at greater than certain tolerated levels. Different smelters have different lists of deleterious elements and different penalty rates for unwanted elements in a copper concentrate (e.g. Lane *et al.*, 2016). Table 4 shows approximate maximum concentrations of deleterious elements that may be present in a copper concentrate before a financial penalty is incurred. Many mining operations therefore work hard to separate deleterious elements from their final saleable concentrate or seek to blend ores from different sources.

Integral to any approach to reducing the concentrations of potential penalty elements in a concentrate is an understanding of the mineralogical hosts for each element in primary ore. As the copper minerals collected from a froth flotation circuit are usually the final saleable copper concentrate (Zanetell, 2007), the concentration of deleterious elements in a concentrate generated

https://doi.org/10.1180/minmag.2017.081.021 Published online by Cambridge University Press

TABLE 4. Copper concentrate deleterious elements.

Deleterious element	Approximate limit in concentrate before charge is incurred (ppm)
Co + Ni	5000
Zn	30,000
As	1000–2000
Se	500
Cd	200
Sb	1000
Hg	10
Pb	10,000
Bi	200–500

Data from Zanetell (2007) and Fountain (2013).

from a chalcopyrite-dominant ore will be related directly to the concentration of deleterious elements within chalcopyrite. Ordinarily, chalcopyrite hosts low enough concentrations of most penalty elements as to not be a significant contributor of such elements in a final copper concentrate. On the basis of the data presented here, only in exceptional circumstances could chalcopyrite itself be expected to contribute to excessive Co, Zn, As, Cd, Sb, Pb and Bi in a copper concentrate. Grains of, for example, arsenopyrite, enargite or tennantite (for As), tetrahedrite (for Sb), galena (for Pb) and Bi-chalcogenides (for Bi) could be considered the likely 'culprits', and efforts may be made to prevent flotation of these minerals.

Chalcopyrite can, however, potentially host sufficient Se or Hg to be a culpable host. Copper concentrates may incur monetary penalties from the smelter if they contain in excess of 500 ppm Se. We measured Se concentrations in chalcopyrite up to 1000 ppm, which could potentially produce copper concentrates with high Se that is difficult to remove prior to smelting. Mercury may represent an even more serious problem in chalcopyrite-dominant copper concentrates. A number of chalcopyrite samples analysed here contain more Hg than the smelter limit of 10 ppm; we even measured hundreds of ppm Hg in chalcopyrite. Japanese smelters charge additional monetary penalties for every 1 ppm over the 10 ppm Hg limit while the Chinese government has banned the import of copper concentrates that exceed 100 ppm Hg altogether (Fountain, 2013). This renders concentrates produced from a Hg-rich chalcopyrite ore of limited value, or in the worst case, unsaleable.

Conclusions

Chalcopyrite may host a wide range of trace elements including Mn, Co, Zn, Ga, Se, Ag, Cd, In, Sn, Sb, Hg, Tl, Pb and Bi. The readiness of chalcopyrite to host trace elements generally increases in the absence of other co-crystallizing sulfides, particularly sphalerite and galena.

In deposits that have recrystallized sulfide assemblages, the concentration of Sn and Ga in chalcopyrite will generally increase in the presence of co-recrystallizing sphalerite and/or galena.

Trace-element concentrations in chalcopyrite typically show little variation at the sample scale, yet there is potential for significant variation between samples from any individual deposit.

The Zn:Cd ratio in chalcopyrite shows systematic variation that depends, in part, on crystallization temperature.

Under constant physiochemical conditions (e.g. temperature, f_{S_2}, pH), the Cd:Zn ratios in co-crystallizing chalcopyrite and sphalerite are typically approximately equal. A distinct difference in the Cd:Zn ratios, and/or a non-constant chalcopyrite Cd:Zn ratio, may indicate varying conditions.

Chalcopyrite is generally a poor host of most penalty elements, Exceptions are Se and Hg, which can be sufficiently enriched in, and difficult to remove from, chalcopyrite-dominant copper concentrates.

Acknowledgements

Benjamin Wade, Aoife McFadden and Ken Neubauer (Adelaide Microscopy) are thanked for their support with analysis. We are grateful to Dominique Tanner, James Day and an additional anonymous reviewer whose insights helped improve this manuscript.

Supplementary material

To view supplementary material for this article, please visit https://doi.org/10.1180/minmag.2017.081.021

References

Andersen, J.C.Ø., Stickland, R.J., Rollinson, G.K. and Shail, R.K. (2016) Indium mineralisation in SW England: Host parageneses and mineralogical relations. *Ore Geology Reviews*, **78**, 213–238.

Ayres, R.U., Ayres, L.W. and Råde, I. (2013) The Life Cycle of Copper; its Co-Products and Byproducts. *Eco-Efficiency in Industry and Science*, **Vol. 13**. Kluwer Academic Publishers, Dordrecht, 199 pp.

Bajwah, Z., Seccombe, P. and Offler, R. (1987) Trace element distribution, Co: Ni ratios and genesis of the

Big Cadia iron-copper deposit, New South Wales, Australia. *Mineralium Deposita*, **22**, 292–300.

Barnes, S.J. and Ripley, E.M. (2016) Highly siderophile and strongly chalcophile elements in magmatic ore deposits. Pp. 725–774 in: *Highly Siderophile and Strongly Chalcophile Elements in High-Temperature Geochemistry and Cosmochemistry* (J. Harvey and J. M.D. Day, editors). Reviews in Mineralogy & Geochemistry, **81**. Mineralogical Society of American and the Geochemical Society, Chantilly, Virginia, USA.

Barnes, S.J., Cox, R.A. and Zientek, M.L. (2006) Platinum-group element, gold, silver and base metal distribution in compositionally zoned sulfide droplets from the Medvezky Creek Mine, Noril'sk, Russia. *Contributions to Mineralogy and Petrology*, **152**, 187–200.

Barrie, C.D., Boyle, A.P., Cook, N.J. and Prior, D.J. (2010) Pyrite deformation textures in the massive sulfide ore deposits of the Norwegian Caledonides. *Tectonophysics*, **483**, 269–286.

Belousov, I., Large, R.R., Meffre, S., Danyushevsky, L.V., Steadman, J. and Beardsmore, T. (2016) Pyrite compositions from VHMS and orogenic Au deposits in the Yilgarn Craton, Western Australia: Implications for gold and copper exploration. *Ore Geology Reviews*, **79**, 474–499.

Bethke, P.M. and Barton, P.B. (1971) Distribution of some minor elements between coexisting sulphide minerals. *Economic Geology*, **66**, 140–163.

Blackburn, W.H. and Schwendeman, J.F. (1977) Trace-element substitution in galena. *Canadian Mineralogist*, **15**, 365–373.

Both, R.A., McElhinney, R. and Toteff, S. (1995) The Angas Zn-Pb-Ag deposit in the Kanmantoo Group, South Australia: synsedimentary or metamorphic? Pp. 847–850 in: *Mineral Deposits: From their origin to their Environmental Impacts* (J. Pasava, B. Kríbek and K. Zák, editors). A. A. Balkema, Rotterdam.

Brill, B. (1989) Trace-element contents and partitioning of elements in ore minerals from the CSA Cu–Pb–Zn deposit, Australia. *Canadian Mineralogist*, **27**, 263–274.

Butler, I.B. and Nesbitt, R.W. (1999) Trace element distributions in the chalcopyrite wall of a black smoker chimney: insights from laser ablation inductively coupled plasma mass spectrometry (LA–ICP–MS). *Earth and Planetary Science Letters*, **167**, 335–345.

Cabri, L.J., Campbell, J.L., Laflamme, J.H.G., Leigh, R.G., Maxwell, J.A. and Scott, J.D. (1985) Proton-microprobe analysis of trace elements in sulfides from some massive-sulfide deposits. *Canadian Mineralogist*, **23**, 133–148.

Chen, L.M., Song, X.Y., Danyushevsky, L.V., Wang, Y.S., Tian, Y.L. and Xiao, J.F. (2014) A laser ablation ICP-MS study of platinum-group and chalcophile elements in base metal sulfide minerals of the Jinchuan Ni-Cu sulfide deposit, NW China. *Ore Geology Reviews*, **65**, 955–967.

Cioacă, M.E., Munteanu, M., Qi, L. and Costin, G. (2014) Trace element concentrations in porphyry copper deposits from Metaliferi Mountains, Romania: A reconnaissance study. *Ore Geology Reviews*, **63**, 22–39.

Ciobanu, C.L., Cook, N.J. and Ivascanu, P. (2001) ore deposits of the Vorţa-Dealul Mare area, South Apuseni Mts., Romania: Textures and a revised genetic model. *ABCD-Geode* 2001. *Romanian Journal of Mineral Deposits*, **79**, 46–47.

Ciobanu, C.L., Cook, N.J. and Stein, H. (2002) Regional setting and geochronology of the Late Cretaceous banatitic magmatic and metallogenetic belt. *Mineralium Deposita*, **37**, 541–567.

Cioflica, G. and Vlad, S. (1981) Cupriferous mineralization at Ciclova. *An Universitatea din Bucuresti Serie de Geologie*, **30**, 1–17.

Cioflica, G., Vlad, S. and Stoici, S. (1971) Repartition de la mineralisation dans les skarns de Baita Bihorului. *Revue Roumaine de Geologie, Geophysique et Geographie, Serie de Geologie*, **15**, 43–58.

Cioflica, G., Vlad, S., Volanschi, E. and Stoici, S. (1977) Magnesian skarns and associated mineralization at Baita Bihor. *Studii şi Cercetări de Geologie, Geofizică şi Geografie, s. Geologie*, **22**, 39–57.

Constantinescu, E., Ilinca, G. and Ilinca, A. (1988) Laramian hydrothermal alteration and ore deposition in the Oravita-Ciclova area. Southwestern Banat. *Dări de Seamă, Institutul Geologic Geofizica*, **72–73**, 13–26.

Cook, N.J. (1992) Antimony-rich mineral parageneses and their association with Au minerals within massive sulphide deposits at Sulitjelma, Norway. *Neues Jahrbuch für Mineralogie Monatsheft*, **3**, 97–106.

Cook, N.J. (1994) Post-recrystallisation phenomena in metamorphosed stratabound sulphide ores: a comment. *Mineralogical Magazine*, **58**, 480–484.

Cook, N.J. (1996) Mineralogy of the sulphide deposits at Sulitjelma, northern Norway. *Ore Geology Reviews*, **11**, 303–338.

Cook, N.J. (2001) Ore mineralogical investigation of the Mofjell deposit (Mo i Rana, Nordland, Norway) with emphasis on gold and silver distribution. *Norges Geologiske Undersøkelse Report* 2001.051, **31**.

Cook, N.J. and Damian, G.S. (1997) New data on "plumosite" and other sulphosalt minerals from the Herja hydrothermal vein deposit, BaiaMare district, Rumania. *Geologica Carpathica*, **48**, 387–399.

Cook, N.J., Halls, C. and Kaspersen, P.O. (1990) The geology of the Sulitjelma ore field, Northern Norway – some new interpretations. *Economic Geology*, **85**, 1720–1737.

https://doi.org/10.1180/minmag.2017.081.021 Published online by Cambridge University Press

Cook, N.J., Halls, C. and Boyle, A.P. (1993) Deformation and metamorphism of massive sulphides at Sulitjelma, Norway. *Mineralogical Magazine*, **57**, 67–81.

Cook, N.J., Spry, P.G. and Vokes, F.M. (1998) Mineralogy and textural relationships among sulphosalts and related minerals in the Bleikvassli Zn-Pb-(Cu) deposit, Nordland, Norway. *Mineralium Deposita*, **34**, 35–56.

Cook, N.J., Ciobanu, C.L., Pring, A., Skinner, W., Shimizu, M., Danyushevsky, L., Saini-Eidukat, B. and Melcher, F. (2009) Trace and minor elements in sphalerite: A LA-ICP-MS study. *Geochimica et Cosmochimica Acta*, **73**, 4761–4791.

Cook, N.J., Ciobanu, C.L., Danyushevsky, L.V. and Gilbert, S. (2011) Minor and trace elements in bornite and associated Cu–(Fe)-sulfides: A LA-ICP-MS study. *Geochimica et Cosmochimica Acta*, **75**, 6473–6496.

Cook, N.J., Ciobanu, C.L. and Ehrig, K. (2015) Insights into zonation within the olympic Dam Cu-U-Au-Ag deposit from trace element signatures of sulfide minerals. *Abstract, SEG 2015 Conference, Hobart, Tasmania, Australia.* Society of Economic Geologists.

Cook, N., Ciobanu, C.L., George, L., Zhu, Z.Y., Wade, B. and Ehrig, K. (2016) Trace element analysis of minerals in magmatic-hydrothermal ores by laser ablation inductively-coupled plasma mass spectrometry: Approaches and opportunities. *Minerals*, **6**, 111.

Danyushevsky, L., Robinson, P., Gilbert, S., Norman, M., Large, R., McGoldrick, P. and Shelley, M. (2011) Routine quantitative multi-element analysis of sulphide minerals by laser ablation ICP-MS: Standard development and consideration of matrix effects. *Geochemistry: Exploration, Environment, Analysis*, **11**, 51–60.

Dare, S.A., Barnes, S.J., Prichard, H.M. and Fisher, P.C. (2010) The timing and formation of platinum-group minerals from the Creighton Ni-Cu-platinum-group Element sulfide deposit, Sudbury, Canada: Early crystallization of PGE-rich sulfarsenides. *Economic Geology*, **105**, 1071–1096.

Demir, Y., Uysal, I., Burhan Sadiklar, M. and Sipahi, F. (2008) Mineralogy, mineral chemistry, and fluid inclusion investigation of Köstere hydrothermal vein-type deposit (Gümüşhane, NE-Turkey). *Neues Jahrbuch für Mineralogie-Abhandlungen: Journal of Mineralogy and Geochemistry*, **185**, 215–232.

Demir, Y., Uysal, İ. and Sadıklar, M.B. (2013) Mineral chemical investigation on sulfide mineralization of the Istala deposit, Gümüşhane, NE-Turkey. *Ore Geology Reviews*, **53**, 306–317.

Djon, M.L.N. and Barnes, S.J. (2012) Changes in sulfides and platinum-group minerals with the degree of alteration in the Roby, Twilight, and High Grade Zones of the Lac des Iles Complex, Ontario, Canada. *Mineralium Deposita*, **47**, 875–896.

Donnay, G., Corliss, L.M., Donnay, J.D.H., Elliott, N. and Hastings, J.M. (1958) Symmetry of magnetic structures: magnetic structure of chalcopyrite. *Physical Review*, **112**, 1917–1923.

Dragov, P. and Petrunov, R. (1996) Elazite porphyry copper-precious metals (Au and PGE) deposit. Pp. 171–175 in: *Proceedings, Annual Meeting of IGCP Project 356, Sofia, Bulgaria*. International Geological Correlation Programme.

Duran, C.J., Barnes, S.J. and Corkery, J.T. (2015) Chalcophile and platinum-group element distribution in pyrites from the sulfide-rich pods of the Lac des Iles Pd deposits, Western Ontario, Canada: Implications for post-cumulus re-equilibration of the ore and the use of pyrite compositions in exploration. *Journal of Geochemical Exploration*, **158**, 223–242.

Eugster, H.P. (1986) Minerals in hot water. *American Mineralogist*, **71**, 655–673.

Flood, B. (1967) Sulphide mineralizations within the Hecla Hoek complex in Vestspitsbergen and Bjørnøya. *Norsk Polarinstitutt Årbok*, **1967**, 109–127.

Foord, E.E. and Shawe, D.R. (1989) The Pb–Bi–Ag–Cu–(Hg) chemistry of galena and some associated sulfosalts: a review and some new data from Colorado, California and Pennsylvania. *Canadian Mineralogist*, **27**, 363–382.

Fountain, C. (2013) The whys and wherefores of penalty elements in copper concentrates. Pp. 502–518 in: *MetPlant 2013: Metallurgical Plant Design and Operating Strategies*, **Vol. 5**. Australasian Institute of Mining and Metallurgy, Melbourne, Australia.

Gena, K., Chiba, H., Kase, K., Nakashima, K. and Ishiyama, D. (2013) The Tiger Sulfide Chimney, Yonaguni Knoll IV Hydrothermal Field, Southern Okinawa Trough, Japan: The first reported occurrence of Pt–Cu–Fe-bearing bismuthinite and Sn-bearing chalcopyrite in an active seafloor hydrothermal system. *Resource Geology*, **63**, 360–370.

George, L., Cook, N.J., Ciobanu, C.L. and Wade, B.P. (2015) Trace and minor elements in galena: A reconnaissance LA-ICP-MS study. *American Mineralogist*, **100**, 548–569.

George, L.L., Cook, N.J. and Ciobanu, C.L. (2016) Partitioning of trace elements in co-crystallized sphalerite–galena–chalcopyrite hydrothermal ores. *Ore Geology Reviews*, **77**, 97–116.

Georgiev, G. (2008) A genetic model of the Elatsite porphyry copper deposit, Bulgaria. *Geochemistry, Mineralogy and Petrology*, **46**, 143–160.

Geoscience Australia (2015) *Copper Fact Sheet*. Australian atlas of minerals resources, mines and processing centres, Geoscience Australia, Commonwealth of Australia. Viewed 8 September

https://doi.org/10.1180/minmag.2017.081.021 Published online by Cambridge University Press

2016, <http://www.australianminesatlas.gov.au/education/fact_sheets/copper.html>

Gheorghitescu, D. (1975) Mineralogical and geochemical study of formations in the thermal, metasomatic contact at Oravita (Cosovita). *Dări de Seamă, Institutul Geologic Geofizica*, **61**, 59–103.

Godel, B. and Barnes, S.J. (2008) Platinum-group elements in sulfide minerals and the whole rocks of the J-M Reef (Stillwater Complex): Implication for the formation of the reef. *Chemical Geology*, **248**, 272–294.

Goldschmidt, V.M. (1954) Geochemistry. *Soil Science*, **78**, 156.

Gottesmann, W. and Kampe, A. (2007) Zn/Cd ratios in calcsilicate-hosted sphalerite ores at Tumurtijn-Ovoo, Mongolia. *Chemie der Erde – Geochemistry*, **67**, 323–328.

Gotz, A., Damian, G. and Farbas, N. (1990) Contributii la mineralogia bournonitul associat mineralizatiilor din masivul Toroiaga-Baia Borsa. Pp. 467–471 in: *High-Temperature and High Pressure Crystal Chemistry* (R. M. Hazen and R.T. Downs, editors). Reviews in Mineralogy & Geochemistry, **41**. Mineralogical Society of American and the Geochemical Society, Chantilly, Virginia, USA.

Hall, S.R. and Stewart, J.M. (1973) The crystal structure refinement of chalcopyrite, $CuFeS_2$. *Acta Crystallographica Section B: Structural Crystallography and Crystal Chemistry*, **29**, 579–585.

Harris, D.C., Cabri, L.J. and Nobiling, R. (1984) Silver bearing chalcopyrite, a principal source of silver in the Izok lake massive-sulfide deposit: confirmation by electron and proton-microprobe analyses. *Canadian Mineralogist*, **22**, 493–498.

Haydon, R.C. and McConachy, G.W. (1987) The stratigraphic setting of Pb-Zn-Ag mineralization at Broken Hill. *Economic Geology*, **82**, 826–856.

Helmy, H.M., Shalaby, I.M. and Rahman, H.A. (2014) Large-scale metal zoning in a late-Precambrian skarn-type mineralization, Wadi Kid, SE Sinai, Egypt. *Journal of African Earth Sciences*, **90**, 77–86.

Holwell, D.A. and McDonald, I. (2007) Distribution of platinum-group elements in the Platreef at Overysel, northern Bushveld Complex: A combined PGM and LA-ICP-MS study. *Contributions to Mineralogy and Petrology*, **154**, 171–190.

Huston, D.L., Sie, S.H., Suter, G.F., Cooke, D.R. and Both, R.A. (1995) Trace elements in sulfide minerals from eastern Australian volcanic-hosted massive sulfide deposits; Part I, Proton microprobe analyses of pyrite, chalcopyrite, and sphalerite, and Part II, Selenium levels in pyrite; comparison with delta ^{34}S values and implications for the source of sulfur in volcanogenic hydrothermal systems. *Economic Geology*, **90**, 1167–1196.

Huston, D.L., Jablonski, W. and Sie, S.H. (1996) The distribution and mineral hosts of silver in eastern Australian volcanogenic massive sulfide deposits. *Canadian Mineralogist*, **34**, 529–546.

Islamov, F., Kremenetsky, E., Minzer, E. and Koneev, R. (1999) The Kochbulak-Kairagach ore field. *Au, Ag, and Cu deposits of Uzbekistan; Excursion Guidebook* (T. Shayakubov , F. Islamov, A. Kremenetshy and R. Seltmann editors). International Field Conference of IGCP-373, Joint SGA-IAGOD symposium, Excursion B6, IGCP-SGA-IAGOD.

Janković, S. (1990) Types of copper deposits related to volcanic environment in the Bor district, Yugoslavia. *Geologische Rundschau*, **79**, 467–478.

Janković, S., Herrington, R.J. and Kozelj, D. (1998) The Bor and Majdanpek copper–gold deposits in the context of the Bor metallogenic zone (Serbia, Yugoslavia). Pp. 169–178 in: *Porphyry and Hydrothermal Copper and Gold Deposits; A Global Perspective* (T.M. Porter, editors). Conference proceedings. Australian Mineral Foundation, Glenside, South Australia.

Jenner, F.E. and O'Neill, H.St.C. (2012) Major and trace analysis of basaltic glasses by laser-ablation ICP-MS. *Geochemistry Geophysics Geosystems*, **13**, https:doi.org/10.1029/2011GC003890.

Jensen, M.L. and Whittle, A.W.G. (1969) Sulfur isotopes of the Nairne pyrite deposit, South Australia. *Mineralium Deposita*, **4**, 241–247.

Johan, Z. (1988) Indium and germanium in the structure of sphalerite: an example of coupled substitution with copper. *Mineralogy Petrology*, **39**, 211–229.

Kase, K. (1987) Tin-bearing chalcopyrite from the Izumo vein, Toyoha Mine, Hokkaido, Japan. *Canadian Mineralogist*, **25**, 9–13.

Kieft, K. and Damman, A.H. (1990) Indium-bearing chalcopyrite and sphalerite from the Gåsborn area, West Bergslagen, central Sweden. *Mineralogical Magazine*, **54**, 109–112.

Kojima, S. and Sugaki, A. (1985) Phase relations in the Cu–Fe–Zn–S system between 500° and 300 °C under hydrothermal conditions. *Economic Geology*, **80**, 158–171.

Kovalenker, V., Safonov, Y., Naumov, V. and Rusinov, V. (1997) The epithermal gold-telluride Kochbulak deposit (Uzbekistan). *Geology of Ore Deposits*, **39**, 107–128.

Lane, D.J., Cook, N.J., Grano, S.R. and Ehrig, K. (2016) Selective leaching of penalty elements from copper concentrates: A review. *Minerals Engineering*, **98**, 110–121.

Lang, B. (1979) The base metals-gold hydrothermal ore deposits of Baia Mare, Romania. *Economic Geology*, **74**, 1336–1351.

Large, R.R., Danyushevsky, L., Hollit, C., Maslennikov, V., Meffre, S., Gilbert, S., Bull, S., Scott, R., Emsbo, P., Thomas, H., Singh, B. and Foster, J. (2009) Gold and trace element zonation in

https://doi.org/10.1180/minmag.2017.081.021 Published online by Cambridge University Press

pyrite using a laser imaging technique: Implications for the timing of gold in orogenic and Carlin-style sediment-hosted deposits. *Economic Geology*, **104**, 635–668.

Layton-Matthews, D., Peter, J.M., Scott, S.D. and Leybourne, M.I. (2008) Distribution, mineralogy, and geochemistry of selenium in felsic volcanic-hosted massive sulfide deposits of the Finlayson Lake district, Yukon Territory, Canada. *Economic Geology*, **103**, 61–88.

Li, Y., Kawashima, N., Li, J., Chandra, A.P. and Gerson, A.R. (2013) A review of the structure, and fundamental mechanisms and kinetics of the leaching of chalcopyrite. *Advances in Colloid and Interface Science*, **197**, 1–32.

Maslennikov, V.V., Maslennikova, S.P., Large, R.R. and Danyushevsky, L.V. (2009) Study of trace element zonation in vent chimneys from the Silurian Yaman-Kasy volcanic-hosted massive sulfide deposit (Southern Urals, Russia) using laser ablation-inductively coupled plasma mass spectrometry (LA-ICPMS). *Economic Geology*, **104**, 1111–1141.

Maydagán, L., Franchini, M., Lentz, D., Pons, J. and McFarlane, C. (2013) Sulfide composition and isotopic signature of the Altar Cu-Au deposit, Argentina: Constraints on the evolution of the porphyry-epithermal system. *Canadian Mineralogist*, **51**, 813–840.

McClenaghan, S.H., Lentz, D.R., Martin, J. and Diegor, W.G. (2009) Gold in the Brunswick No. 12 volcanogenic massive sulfide deposit, Bathurst Mining Camp, Canada: Evidence from bulk ore analysis and laser ablation ICP─ MS data on sulfide phases. *Mineralium Deposita*, **44**, 523–557.

McDonough, W.F. and Sun, S.S. (1995) The composition of the Earth. *Chemical Geology*, **120**, 223–253.

Mikhlin, Y., Tomashevich, Y., Tauson, V., Vyalikh, D., Molodtsov, S. and Szargan, R. (2005) A comparative X-ray absorption near-edge structure study of bornite, Cu_5FeS_4, and chalcopyrite, $CuFeS_2$. *Journal of Electron Spectroscopy and Related Phenomena*, **142**, 83–88.

Moggi-Cecchi, V., Cipriani, C., Rossi, P., Ceccato, D., Rudello, V. and Somacal, H. (2002) Trace element contents and distribution maps of chalcopyrite: a micro-PIXE study. *Periodico di Mineralogia*, **71**, 101–109.

Monteiro, L.V.S., Xavier, R.P., Hitzman, M.W., Juliani, C., de Souza Filho, C.R. and Carvalho, E.D. R. (2008) Mineral chemistry of ore and hydrothermal alteration at the Sossego iron oxide–copper–gold deposit, Carajás Mineral Province, Brazil. *Ore Geology Reviews*, **34**, 317–336.

Mular, A.L., Halbe, D.N. and Barratt, D.J. (editors) (2002) *Mineral Processing Plant Design, Practice, and Control*. Society for Mining, Metallurgy, and Exploration.

Müller, W., Shelley, M., Miller, P. and Broude, S. (2009) Initial performance metrics of a new custom-designed ArF excimer LA-ICPMS system coupled to a two-volume laser ablation cell. *Journal of Analytical Atomic Spectrometry*, **24**, 209–214.

Parr, J. and Plimer, I. (1993) Models for Broken Hill-type lead-zinc-silver deposits. *Mineral Deposits Modeling. Geological Association of Canada Special Paper*, **40**, 245–288.

Patten, C., Barnes, S.-J., Mathez, E.A. and Jenner, F.E. (2013) Partition coefficients of chalcophile elements between sulfide and silicate melts and the early crystallization history of sulfide liquid: LA-ICP-MS analysis of MORB sulfide droplets. *Chemical Geology*, **358**, 170–188.

Pauling, L. and Brockway, L.O. (1932) The crystal structure of chalcopyrite $CuFeS_2$. *Zeitschrift für Kristallographie – Crystalline Materials*, **82**, 188–194.

Pearce, C.I., Pattrick, R.A.D., Vaughan, D.J., Henderson, C.M.B. and Van der Laan, G. (2006) Copper oxidation state in chalcopyrite: Mixed Cu d^9 and d^{10} characteristics. *Geochimica et Cosmochimica Acta*, **70**, 4635–4642.

Piña, R., Gervilla, F., Barnes, S.J., Ortega, L. and Lunar, R. (2012) Distribution of platinum-group and chalcophile elements in the Aguablanca Ni-Cu sulfide deposit (SW Spain): Evidence from a LA-ICP-MS study. *Chemical Geology*, **302**, 61–75.

Plimer, I.R. (2007) The world's largest Zn-Pb-Ag deposit: a re-evaluation of Broken Hill (Australia). Pp. 1239–1242 in: *Mineral deposits: Digging Deeper* (C.J. Andrew, editors). Irish Association for Economic Geology, Dublin.

Plotinskaya, O.Y., Kovalenker, V., Seltmann, R. and Stanley, C. (2006) Te and Se mineralogy of the high-sulfidation Kochbulak and Kairagach epithermal gold telluride deposits (Kurama Ridge, Middle Tien Shan, Uzbekistan). *Mineralogy and Petrology*, **87**, 187–207.

Popov, P., Strashimirov, S. and Kanazirski, M. (2000) Assarel-Medet ore field. Pp. 19–25 in: *Geology and Metallogeny of the Panagyurishte Ore Region. Guide to Excursion A and C* (S. Strashmirov and P. Popov, editors). ABCD–Geode 2000 Workshop, Borovets, May 2000.

Prichard, H.M., Knight, R.D., Fisher, P.C., McDonald, I., Zhou, M.F. and Wang, C.Y. (2013) Distribution of platinum-group elements in magmatic and altered ores in the Jinchuan intrusion, China: An example of selenium remobilization by postmagmatic fluids. *Mineralium Deposita*, **48**, 767–786.

Reich, M., Palacios, C., Barra, F. and Chryssoulis, S. (2013) "Invisible" silver in chalcopyrite and bornite from the Mantos Blancos Cu deposit, northern Chile. *European Journal of Mineralogy*, **25**, 453–460.

https://doi.org/10.1180/minmag.2017.081.021 Published online by Cambridge University Press

Revan, M.K., Genç, Y., Maslennikov, V.V., Maslennikova, S. P., Large, R.R. and Danyushevsky, L.V. (2014) Mineralogy and trace-element geochemistry of sulfide minerals in hydrothermal chimneys from the Upper-Cretaceous VMS deposits of the eastern Pontide orogenic belt (NE Turkey). *Ore Geology Reviews*, **63**, 129–149.

Rubin, J.N. and Kyle, J.R. (1997) Precious metal mineralogy in porphyry-, skarn-, and replacement-type ore deposits of the Ertsberg (Gunung Bijih) District, Irian Jaya, Indonesia. *Economic Geology*, **92**, 535–550.

Saager, R. (1967) Drei Typen von Kieslagerstätten im Mofjell-Gebiet, Nordland, und ein neuer Vorschlag zur Gliederung der Kaledonischen Kieslager Norwegens. *Norsk Geologisk Tidsskrift*, **47**, 333–358.

Sadati, S.N., Yazdi, M., Mao, J., Behzadi, M., Adabi, M. H., Lingang, X., Zhenyu, C. and Mokhtari, M.A.A. (2016) Sulfide mineral chemistry investigation of sediment-hosted stratiform copper deposits, Nahand-Ivand area, NW Iran. *Ore Geology Reviews*, **72**, 760–776.

Schwartz, M.O. (2000) Cadmium in zinc deposits: economic geology of a polluting element. *International Geology Review*, **42**, 445–469.

Scott, K.M., Ashley, P.M. and Lawie, D.C. (2001) The geochemistry, mineralogy and maturity of gossans derived from volcanogenic Zn–Pb–Cu deposits of the eastern Lachlan Fold Belt, NSW, Australia. *Journal of Geochemical Exploration*, **72**, 169–191.

Seccombe, P.K., Spry, P.G., Both, R.A., Jones, M.T. and Schiller, J.C. (1985) Base metal mineralization in the Kanmantoo Group, South Australia: a regional sulfur isotope study. *Economic Geology*, **80**, 1824–1841.

Serranti, S., Ferrini, V., Masi, U., Nicoletti, M. and Conde, L.N. (2002) Geochemical features of the massive sulfide (Cu) metamorphosed deposit of Arinteiro (Galicia, Spain) and genetic implications. *Periodico di Mineralogia*, **71**, 27–48.

Shalaby, I. M., Stumpfl, E., Helmy, H.M., El Mahallawi, M.M. and Kamel, O.A. (2004) Silver and silver-bearing minerals at the Um Samiuki volcanogenic massive sulphide deposit, Eastern Desert, Egypt. *Mineralium Deposita*, **39**, 608–621.

Shannon, R. (1976) Revised effective ionic radii and systematic studies of interatomic distances in halides and chalcogenides. *Acta Crystallographica Section A*, **32**, 751–767.

Shimizu, M., Cioflica, G. and Lupulescu, M. (1995) Ore mineralogy of Romanian deposits. Part I. Stanija and Baita Bihor, Apuseni Mountains and Tincova-Valisor, Banat (SW Carpathians), Romania. *Japanese Magazine of Mineralogical Petrological Sciences*, **45**, 280–281.

Simon, G., Kesler, S.E., Essene, E.J. and Chryssoulis, S. L. (2000) Gold in porphyry copper deposits: experimental determination of the distribution of gold in the Cu-Fe-S-Au system at 400 to 700 °C. *Economic Geology*, **94**, 259–270.

Smith, J.W., Holwell, D.A., McDonald, I. and Boyce, A.J. (2016) The application of S isotopes and S/Se ratios in determining ore-forming processes of magmatic Ni-Cu-PGE sulfide deposits: A cautionary case study from the northern Bushveld Complex. *Ore Geology Reviews*, **73**, 148–174.

Spry, P.G., Plimer, I.R. and Teale, G.S. (2008) Did the giant Broken Hill (Australia) Zn-Pb-Ag deposit melt? *Ore Geology Reviews*, **34**, 223–241.

Spry, P.G., Both, R.A., Ogierman, J., McElhinney, R. and Heimann, A. (2010) Origin of the Angas Pb-Zn-Ag deposit, Strathalbyn, South Australia. *Society of Economic Geologists SEG 2010 Conference, Keystone, Colorado, Extended Abstract*.

Strashimirov, S. (1993) Features in distribution of the ore minerals in the western periphery of the porphyry-copper deposit Assarel. *Ann HIMG*, **39**, 79–93 [in Bulgarian].

Strashimirov, S., Petrunov, R. and Kanazirski, M. (2002) Porphyry-copper mineralisation in the central Srednogorie zone, Bulgaria. *Mineralium Deposita*, **37**, 587–598.

Subba Rao, D.V. and Naqvi, S.M. (1997) Geological setting, mineralogy, geochemistry and genesis of the Middle Archaean Kalyadi copper deposit, western Dharwar craton, southern India. *Mineralium Deposita*, **32**, 230–242.

Szöke, A. and Steclaci, L. (1962) *Regiunea Toroiaga, Baia-Borsa: studiu geologic, petrografic, mineralogic si geochimic*. Editura Academiei Republicii Populare Romine.

Thole, R.H. (1976) The geology of the Shamrocke mine, Rhodesia – a stratiform copper deposit. *Economic Geology*, **71**, 202–228.

Todd, E.C. and Sherman, D.M. (2003) Surface oxidation of chalcocite (Cu_2S) under aqueous (pH = 2–11) and ambient atmospheric conditions: mineralogy from Cu L-and O K-edge X-ray absorption spectroscopy. *American Mineralogist*, **88**, 1652–1656.

Todd, E.C., Sherman, D.M. and Purton, J.A. (2003) Surface oxidation of chalcopyrite ($CuFeS_2$) under ambient atmospheric and aqueous (pH 2–10) conditions: Cu, Fe L- and O K-edge X-ray spectroscopy. *Geochimica et Cosmochimica Acta*, **67**, 2137–2146.

Ulrich, T., Golding, S.D., Kamber, B.S., Zaw, K. and Taube, A. (2002) Different mineralization styles in a volcanic-hosted ore deposit: the fluid and isotopic signatures of the Mt Morgan Au–Cu deposit, Australia. *Ore Geology Reviews*, **22**, 61–90.

United States Geological Survey (2014) *Microanalytical Reference Materials and Accessories*. United States Geological Survey. Viewed 6 October 2016, <http://crustal.usgs.gov/geochemical_reference_standards/microanalytical_RM.html>

https://doi.org/10.1180/minmag.2017.081.021 Published online by Cambridge University Press

Van Achterbergh, E., Ryan, C., Jackson, S. and Griffin, W. (2001) Data reduction software for LA-ICP-MS. Pp. 239–243 in: Laser-Ablation-ICPMS in the earth sciences – principles and applications. *Mineralogical Association of Canada (short course series)*, **29**.

Verwoerd, P.J. and Cleghorn, J.H. (1975) Kanmantoo copper orebody. Pp. 560–565 in: *Economic Geology of Australia and Papua New Guinea – I Metals* (C.L. Knight, editors). Australasian Institute of Mining and Metallurgy Monograph, **5**.

Vokes, F.M. (1963) Geological studies on the Caledonian pyritic zinc-lead orebody at Bleikvassli, Norland, Norway. *Norges Geologiske Undersøkelse*, **222**, 1–126.

Vokes, F.M. (1966) On the possible modes of origin of the Caledonian sulfide ore deposit at Bleikvassli, Nordland, Norway. *Economic Geology*, **61**, 1130–1139.

Wang, G., Wang, Z.Q., Shi, R., Zhang, Y.L. and Wang, K. M. (2015*a*) Mineralogy and isotope geochemical characteristics for Xiaozhen copper deposit, Langao County, Shaanxi Province and their constraint on genesis of the deposit. *Geosciences Journal*, **19**, 281–294.

Wang, Z., Xu, D., Zhang, Z., Zou, F., Wang, L., Yu, L. and Hu, M. (2015*b*) Mineralogy and trace element geochemistry of the Co-and Cu-bearing sulfides from the Shilu Fe–Co–Cu ore district in Hainan Province of South China. *Journal of Asian Earth Sciences*, **113**, 980–997.

Wilson, S., Ridley, W. and Koenig, A. (2002) Development of sulphide calibration standards for the laser ablation inductively-coupled plasma mass spectrometry technique. *Journal of Analytical Atomic Spectrometry*, **17**, 406–409.

Winderbaum, L., Ciobanu, C.L., Cook, N.J., Paul, M., Metcalfe, A. and Gilbert, S. (2012) Multivariate analysis of an LA-ICP-MS trace element dataset for pyrite. *Mathematical Geosciences*, **44**, 823–842.

Wittmann, A. (1974) Indium. 49-A Crystal Chemistry. In: *Handbook of Geochemistry* (K.H. Wedepohl, editors). Springer-Verlag, Berlin, v. II/4, 49-A-1-49-A-8.

Wohlgemuth-Ueberwasser, C. C., Viljoen, F., Petersen, S. and Vorster, C. (2015) Distribution and solubility limits of trace elements in hydrothermal black smoker sulfides: An in-situ LA-ICP-MS study. *Geochimica et Cosmochimica Acta*, **159**, 16–41.

Zanetell, Z.A. (2007) *Penalty Element Separation from Copper Concentrates Utilizing Froth Flotation*. Masters thesis, Colorado School of Mines, Colorado, USA.

https://doi.org/10.1180/minmag.2017.081.021 Published online by Cambridge University Press